TECHNOLOGY

593
S6R
1.62 no. 4

Journal of Research

of the

National Bureau of Standards

PUBLIC LIBRARY
MAY 11 1959
DETROIT

APRIL 1959

VOLUME 62 NUMBER 4

U.S. DEPARTMENT OF COMMERCE
Lewis L. Strauss, Secretary
NATIONAL BUREAU OF STANDARDS
A. V. Astin, Director

APRIL • 1959
VOLUME • 62
NUMBER • 4

JOURNAL OF RESEARCH
of the
NATIONAL BUREAU OF STANDARDS

The National Bureau of Standards

Functions and Activities

The functions of the National Bureau of Standards are set forth in the Act of Congress, March 3, 1901, as amended by Congress in Public Law 619, 1950. These include the development and maintenance of the national standards of measurement and the provision of means and methods for making measurements consistent with these standards; the determination of physical constants and properties of materials; the development of methods and instruments for testing materials, devices, and structures; advisory services to government agencies on scientific and technical problems; invention and development of devices to serve special needs of the Government; and the development of standard practices, codes, and specifications. The work includes basic and applied research, development, engineering, instrumentation, testing, evaluation, calibration services, and various consultation and information services. Research projects are also performed for other government agencies when the work relates to and supplements the basic program of the Bureau or when the Bureau's unique competence is required. The scope of activities is suggested by the listing of divisions and sections on the inside of the back cover.

Publications

The results of the Bureau's work take the form of either actual equipment and devices or published papers. These papers appear either in the Bureau's own series of publications or in the journals of professional and scientific societies. The Bureau itself publishes three monthly periodicals, available from the Government Printing Office: The Journal of Research, which presents complete papers reporting technical investigations; the Technical News Bulletin, which presents summary and preliminary reports on work in progress; and Basic Radio Propagation Predictions, which provides data for determining the best frequencies to use for radio communications throughout the world. There are also five series of nonperiodical publications: The Applied Mathematics Series, Circulars, Handbooks, Building Materials and Structures Reports, and Miscellaneous Publications.

Information on the Bureau's publications can be found in NBS Circular 460, Publications of the National Bureau of Standards ($1.25) and its Supplement ($1.50), available from the Superintendent of Documents, Government Printing Office, Washington 25, D.C.

Order all publications from the Superintendent of Documents
U.S. Government Printing Office, Washington 25, D.C.

Use of funds for printing this publication approved by the Director of the Bureau of the Budget (June 24, 1958)

Journal of Research of the National Bureau of Standards Vol. 62, No. 4, April 1959 Research Paper 2943

Interferometer for Large Surfaces

James B. Saunders and Franz L. Gross[1]

An interferometer is described that permits the testing of large areas, such as layout plates. The extension to large areas is obtained by causing a collimated beam of light to reflect from the specimen at a large angle of incidence. The resultant fringe pattern is a contour map of the surface relative to an arbitrarily chosen plane and the contour interval is a function of wavelength and angle of incidence.

1. Introduction

An interferometer for testing large surfaces has been described by Linnik.[2] However, in spite of certain advantages, the Linnik interferometer has not been used extensively in this country. This lack of application may be due to the complexity of the instrument.

The instrument described here is relatively simple and easy to operate, is twice as sensitive as the Linnik interferometer, and is relatively free from vibrations.

2. Optics of the Interferometer

The optics of this interferometer are shown schematically in figure 1. The light from a source at S is collimated by the lens L_1, and separated into two coherent beams by the semireflecting dividing plane of a Kösters double image prism.[3,4] The entrance angle of the collimated light may be adjusted to give any desired deviation θ between the component beams 1 and 2. Beam 1 is reflected normally from mirror M_1 and returns upon itself. Beam 2 is reflected from the surface to be tested at an angle of incidence of $90-\beta$ degrees, then normally from mirror M_2 and returns along its previous path to the dividing plane of the prism, where it recombines with beam 1. The observer at E sees interference fringes on the superimposed images of the two mirrors.

The gross aspects of the fringe pattern (fringe direction and spacing) are controlled by the wedge angle between the wave fronts of beams 1 and 2, while the small irregularities of the fringe pattern are a function of the irregularities of the test surface. If the test surface were perfectly flat, the fringes would be straight and parallel. Any curvature of the test surface introduces a corresponding curvature in the wave front of beam 2, and this wave front, when compared with the plane wave front of beam 1, introduces curvature into the otherwise straight fringes. By adjusting the tilt of the test surface (i.e., setting $\beta=\theta$ and introducing a slight tilt across the width of the test area), it is possible to adjust the fringes so that they run parallel to the long dimension of the test area (as seen by the observer at E). In this case, the curvature of the fringes is a direct and precise measure of the curvature of the test area (in its long dimension). The fringe pattern is a contour map of the area of the specimen surface that is being tested.

3. Sensitivity

The sensitivity of the instrument depends upon the value of β. Since the light is reflected twice from the specimen surface, the sensitivity is double that obtained with the Linnik interferometer for the same angle of incidence. When the instrument is adjusted as described in the preceding section, one fringe departure from straightness corresponds to a departure from flatness of $\lambda/(4 \sin \beta)$, where λ is the wavelength of light.

[1] Present address: University College, London, England.
[2] V. P. Linnik, Compt. rend. acad. sci. U.R.S.S. **35,** 16 (1942).
[3] J. B. Saunders, Construction of a Kösters double-image prism, J. Research NBS, **58,** 21 (1957) RP2729.
[4] The Kösters double image prism is made from two 30°-60°-90° prisms, one of which is partially silvered on the face opposite the 60° angle. The two prisms are then cemented together to form the equilateral prism shown in figure 1. The partially silvered surface becomes a semireflecting plane.

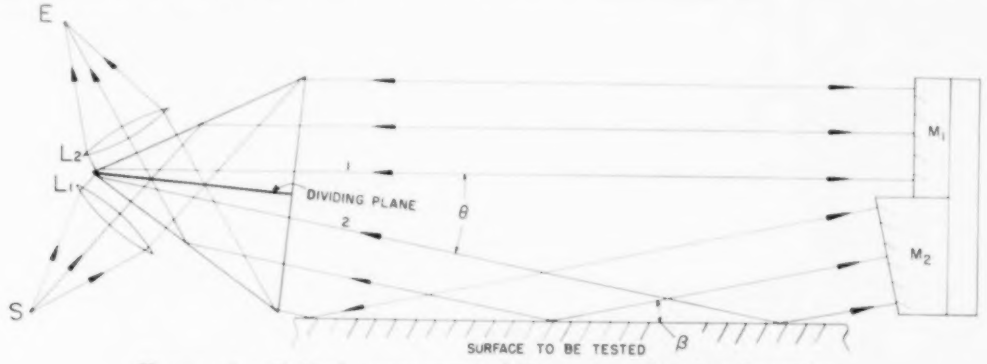

FIGURE 1. *Optical arrangement of the surface plate interferometer.*

In a finished instrument, the angles θ and β could be made adjustable so that any length surface could be made to fill the aperture of the system. This would give maximum sensitivity for any size surface measured. However, since the value of β must be known for evaluating the fringe pattern, it may be more practical to use fixed values for θ and β (with M_1 and M_2 bound into a rigid unit) and bind the mirror unit to the prism housing. This would eliminate the necessity of making frequent measurements of β and also add stability to the instrument. The resulting instrument would have a fixed adjustment and could be used by an unskilled operator.

The maximum length of surface that may be covered with one setting is $A \csc \beta$, where A is the aperture of the prism. Thus by decreasing β, any length surface could be covered with a prism of a given aperture, but of course the sensitivity of the instrument would also decrease.

4. Experimental Model

Figure 2 is a photograph of the pilot model that was used to test the interferometer. The surface plate used in this assembly was 91 cm long. The wedge angle between the wave fronts was controlled by adjusting the end mirrors, which produced the same effect as tilting the surface plate. The Kösters double image prism and lens assembly shown in figure 2 were taken from another instrument that was designed for use with a clear circular aperture of

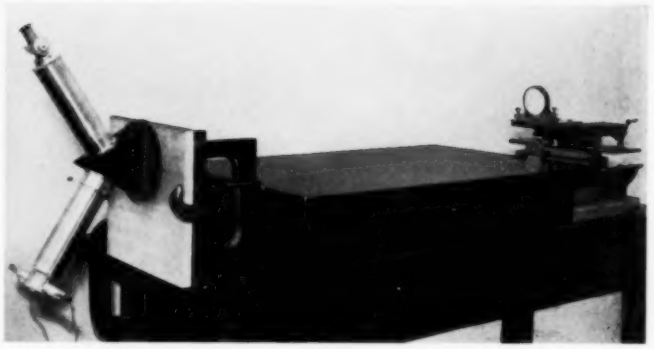

FIGURE 2. *Pilot model of surface plate interferometer for testing feasibility of the optical principals with a typical granite surface plate.*

The reflectivity of the end mirrors is designed to give approximately equal intensity for the two lightbeams at the receiving point E.

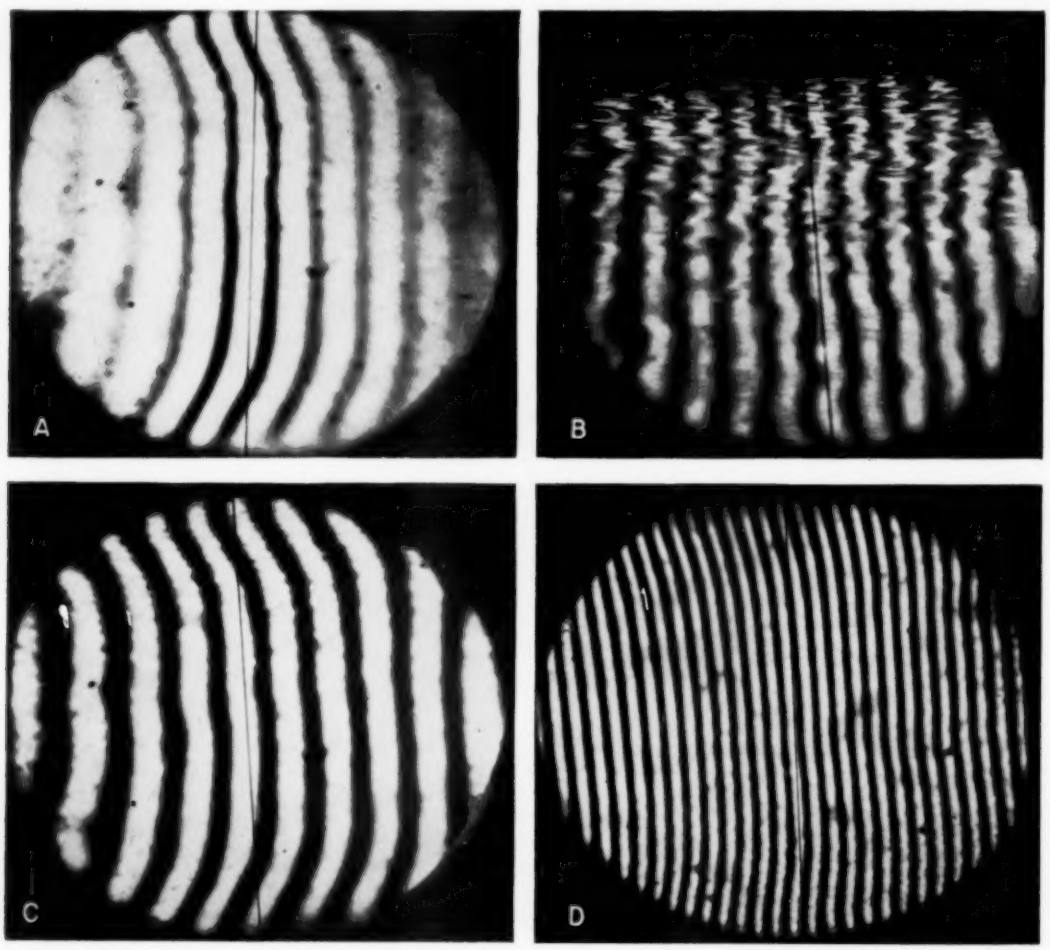

FIGURE 3. *Fringe patterns.*

A, White light from granite surface plate; B, monochromatic light from a badly scratched cast iron surface; C and D, monochromatic light from a granite surface. Angle of incident on surface plate is approximately $2\frac{1}{2}°$.

51-mm diam (2 in.).[5] Since the prism had an aperture 51-mm square, better coverage of the specimen surface could have been obtained by increasing the circular aperture to $51\sqrt{2}$ mm. This would have left the square aperture of the prism unobstructed, so that the area of the specimen being tested would have been a rectangle 51 mm by 91 cm, and the unfavorable narrowing of the field at the ends of the specimen due to the circular aperture would have been eliminated.

5. Results

The interference fringes shown in figure 3 were taken with the instrument described above and shown in figure 2. Photograph A was made with white light and the others with monochromatic (λ=5876 A) light. The difference between photographs C and D was obtained by changing the angle between the two interfering wavefronts, thus changing the width of the fringes. Photographs A, C, and D of figure 3 were made with the plate of black granite, shown in figure 2, whereas photograph B was made with an old cast iron plate (dated 1918) that was badly scratched and marred. In this model the angle β was 2½° and thus a departure from straightness of one fringe corresponds to a deviation from flatness of 5.75 λ (approximately 0.00013 in.).

The optical performance of this instrument was found to be highly satisfactory. Some mechanical development is necessary in order to produce a more practical instrument. Accordingly, a few suggestions given here may be of help to the designer. The prism should be designed to use its entire rectangular aperture. The apertures of the lenses should be sufficiently large to prevent constriction of this aperture. The prism and end mirrors should be rigidly bound together if vibrations of the fringes are to be avoided. White light may be used but the resulting difficulty of finding and adjusting the fringes exceeds the inconveniences associated with monochromatic sources.

[5] This prism assembly was designed for use with θ=0°. Using it at θ=2½°, the circular aperture became an oval aperture with a vertical diameter of 45 mm.

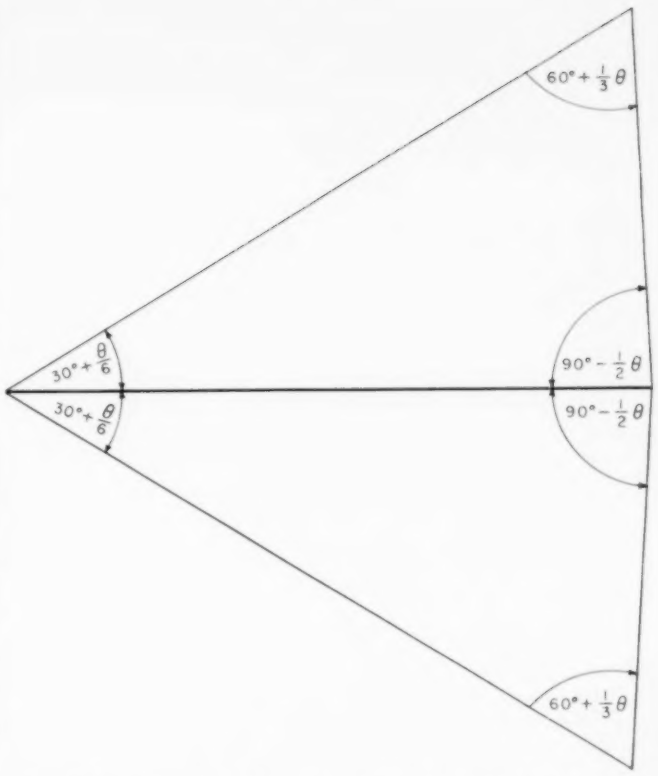

FIGURE 4. *Modified Kösters double-image prism for use with monochromatic light.*

A cover that encloses the light beams, between the prism and end mirrors, greatly enhances the stability of the fringes, and should be used unless the surrounding air is in a steady state. If white light is to be used, differential refraction may be reduced to a minimum by using the form of Kösters prism shown in figure 4. The procedure for making such a prism differs from that described in footnote 4 in that all surfaces are finished before cutting the prism into two parts.

WASHINGTON, December 8, 1959.

Journal of Research of the National Bureau of Standards Vol. 62, No. 4, April 1959 Research Paper 2944

Glass Formation in Polymers: II. The System Rubber-Sulfur

Gordon M. Martin and Leo Mandelkern

Volume versus temperature relations encompassing a wide range in temperature and composition have been determined for a series of natural rubber-sulfur vulcanizates and mixtures. The characteristic temperature of glass formation is deduced from these studies. The glass temperature is found to increase continuously from −69° to +90° C in the vulcanizates as the amount of bound sulfur is increased and to be invariant with the composition in the mixtures. A qualitative interpretation of these results is given in terms of the free-volume theory of glass formation.

1. Introduction

The physical and mechanical properties of bulk amorphous polymers depend to a large extent on the relationship between the temperature of study and the temperature at which glass formation occurs. Thus at temperatures above that for glass formation amorphous polymers exhibit rubberlike elastic behavior, while at temperatures below the transformation temperature brittle inelastic behavior is observed. This phenomenon is exemplified in a remarkable fashion by sulfur vulcanizates of natural rubber. For this system, at room temperature, normal rubberlike behavior is observed when relatively small amounts of sulfur have reacted. On the other hand, as the amount of bound sulfur increases the polymer becomes hard and inelastic. It is, of course, well known that with the increase in the amount of combined sulfur the glass temperature, T_g, increases from −69° to temperatures which are well above room temperature [1][1] and it is this fact that causes the observed changes in physical properties.

Glass formation occurs as a consequence of the fact that as the temperature or pressure is varied the time necessary for molecules or segments of molecules to rearrange from one local liquid equilibrium structure to another becomes comparable with, or greater than, the time scale of the experimental observations [2, 3]. One important problem has been that of being able to quantitatively describe the variation of T_g of a given polymer with structural or compositional changes that are introduced. A great deal of success has been achieved in solving this general problem by considering the changes that occur in the free volume of the system as a result of the alteration of the structure or composition [3 to 7]. Based on the theory of activated processes, the free volume can be considered to be a measure of the ease with which the necessary molecular rearrangements occur. Furthermore, the variation of the free volume should be intimately related to the changes that occur in the specific volume of the system.

The earlier work of McPherson [8] and Scott [9] indicates that one consequence of the reaction of sulfur and natural rubber is a significant and systematic change in the density of the system. These results give indication that the change that occurs in T_g might be explicable by considering the variation of the specific volume of the system with temperature and composition. The data reported, however, do not cover a sufficiently wide range in temperature to be suited for this purpose. Thus there is no complete set of data available which describe the variation of T_g with composition and give the specific volume-temperature relations for the same series of compounds over a wide composition range.

The present work was undertaken to investigate this problem more thoroughly. Detailed studies of the volume-temperature relations of purified natural rubber, natural rubber-sulfur mixtures, and of vulcanizates of these two substances, encompassing the completely accessible composition range and covering a very wide range in temperatures, were made. The present paper discusses the variation of T_g with composition in both the mixtures and vulcanizates and interprets it in terms of the changes that occur in the specific volume of the system.

2. Experimental Procedures

2.1. Materials

The natural rubber used in this study was a sample of smoked sheet, technically classified yellow. This sample was purified by extracting with acetone for 8 days; it was then dried in vacuum, and 1.25 percent of phenyl-β-naphthylamine was added as an antioxidant. Two master samples containing 30 percent and 32 percent sulfur by weight were prepared by mixing the rubber and sulfur on a small mill. The other mixtures and samples for vulcanization were prepared on the mill by adding an appropriate amount of the purified rubber to one of the master samples.

The vulcanization was accomplished by curing in a conventional press for 20 hr at 150° C. Eighteen vulcanizates of varying compositions were prepared, and the order of preparation and measurement of

[1] Figures in brackets indicate the literature references at the end of this paper.

their respective physical properties was randomized so that any slow oxidative processes which might occur during storage would not bias the results. To further minimize oxidation and degradation all of the rubber samples were stored in a solid-carbon dioxide chest. The unreacted mixtures of the rubber and sulfur were prepared by pressing in a vacuum mold at 100° C prior to their physical examination. The percentage of sulfur chemically bound in the vulcanizates was determined by analysis after the removal of free sulfur by acetone extractions. The method of analysis was a micro Carius combustion followed by the gravimetric determination of the sulfur as barium sulfate.[2] It was found that the percentage of bound sulfur was usually less than the sulfur contained in the mixtures prior to vulcanization.

2.2. Methods

The linear thermal expansion of the mixtures and of the vulcanizates was determined by using a photoelectric recording interferometer. The design and operation of this instrument have been described by Work [10]. He concluded that T_g can be measured with a precision of $\pm 1.0°$ C with this instrument and that the coefficients of linear expansions are reproducible within ± 5 percent.

In making these measurements three specimens about 5 by 5 by 3 mm were cut from each sample and used as spacers between the two quartz optical flats. The specimens were first heated in the interferometer to the maximum temperature to be used, then several runs on both heating and cooling cycles were made. The heating was done electrically and the cooling by liquid nitrogen. The rate of temperature change was about 1° C per minute and a temperature interval from −180° to +140° C was studied.

The record from the photoelectric recording interferometer gives thermocouple emf horizontally as a measure of temperature and a vertical step for each fringe or half wavelength change in thickness of the specimens. The linear expansion at any temperature T can be found from this record by means of the equation:

$$\Delta L/L_0 = N\lambda/2L_0 + C \qquad (1)$$

The temperature T is determined from the thermocouple emf; ΔL is the change in length between the reference temperature T_0 and T; L_0 is the average thickness of the specimens at T_0 (25° C in the present work); N is the number of fringes between T_0 and T; λ is the wavelength of the light used in air at temperature T_0; and C is a factor correcting for the change in wavelength in air with temperature. The values of C at various temperatures for the helium yellow light ($\lambda = 5876$ A) used are given by Merritt [11].

In interpreting the experimental results, it is more convenient to consider the specific volume and its changes with temperature rather than the change in length. To accomplish this conversion the specific volume v at temperature T was calculated from the linear expansion by the relation

$$v = v_0(1 + \Delta L/L_0)^3 \qquad (2)$$

where v_0 is the specific volume at a reference temperature T_0. This relation is exact when the expansion is isotropic. This assumption appears to be well founded for amorphous polymers, and the volume expansion calculated from interferometric data compares well with the direct determination of this quantity by dilatometric means [12]. The specific volumes of the samples were determined at 25° C by the method of hydrostatic weighing [13].

3. Results

The volume-temperature relations, determined in the described manner, for the series of rubber-sulfur vulcanizates encompassing a composition range of 0 to 30 percent bound sulfur are plotted in figure 1. The curve pertinent to a specific vulcanizate is designated by a number corresponding to the percent bound sulfur. The glass temperature T_g is taken at the point of intersection of the two straight lines which represent the volume-temperature coefficient in the liquid and in the glassy state. Above T_g the volume-temperature data are well represented by a linear relation. However, below T_g the linear region covers only a very small temperature interval and the data are best represented by a curve of decreasing slope with decreasing temperature, as has been observed in other polymeric systems [7, 12]. Although for this reason a precise determination of T_g is difficult, values which are reliable on a comparative basis can be easily obtained.

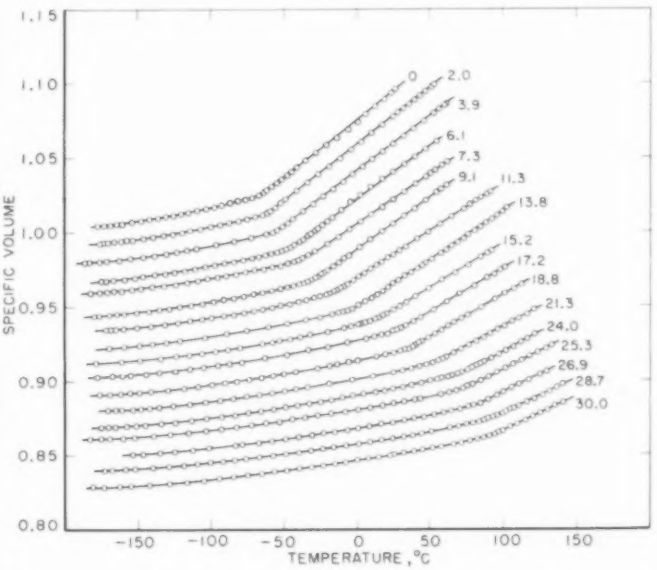

FIGURE 1. *Plot of specific volume as function of temperature for each of the rubber-sulfur vulcanizates.*

Number on right indicates percent bound sulfur.

[2] The chemical analysis was performed by R. A. Paulson and Miss L. J. Tregoning of the National Bureau of Standards.

Values of T_g for the various rubber-sulfur vulcanizates are listed in the fifth column of table 1. For this series of compounds T_g continuously increases as the combined sulfur content is increased, ranging from −69° C for the pure natural rubber to +90° C for the sample containing 30 percent sulfur. Thus a very wide range in glass temperatures can be achieved merely by reacting an appropriate quantity of sulfur with natural rubber. The manner in which T_g changes with sulfur composition is illustrated in figure 2. The curve in this figure is distinctly S-shaped since the initial amounts of bound sulfur cause only a relatively slight rise in T_g. However, when about 4 percent sulfur has been combined the rate of increase accelerates and finally levels off at the higher sulfur contents. The general shape of the curve in figure 2 is similar to that given by Boyer and Spencer [1] where values of T_g as a function of sulfur content, determined by a wide variety of methods, were collected from the then existing literature. A similar plot is also given by Schmieder and Wolf [14] where the values of T_g were determined by dynamical mechanical methods. In the latter work the values of T_g are significantly higher over the complete composition range than those reported here, while the compilation of Boyer and Spencer appears to be in good agreement with the present work except at the very highest sulfur contents where the literature values appear to be about 10° lower.

In figure 1 the volume-temperature curves depicting each of the compounds are displaced to lower values as the sulfur content is increased. Thus at a reference temperature either in the liquid state or in the glassy state the specific volume decreases with increasing sulfur content. This decrease in specific volume and the concomitant increase in T_g is similar to that which is observed in many other polymeric systems [3, 7]. Taking 25° C as a reference temperature in the liquid state, the specific volumes corresponding to this temperature are given in table 1 and are also plotted in figure 3. For those systems which are actually in the glassy state at the reference temperature the appropriate values of the specific volume were obtained by a linear extrapolation of the liquidus. From figure 3 it can be seen that the specific volumes of the vulcanizates at the reference temperature decrease linearly with composition until about 19 percent sulfur at which point the rate of decrease of the specific volume becomes appreciably

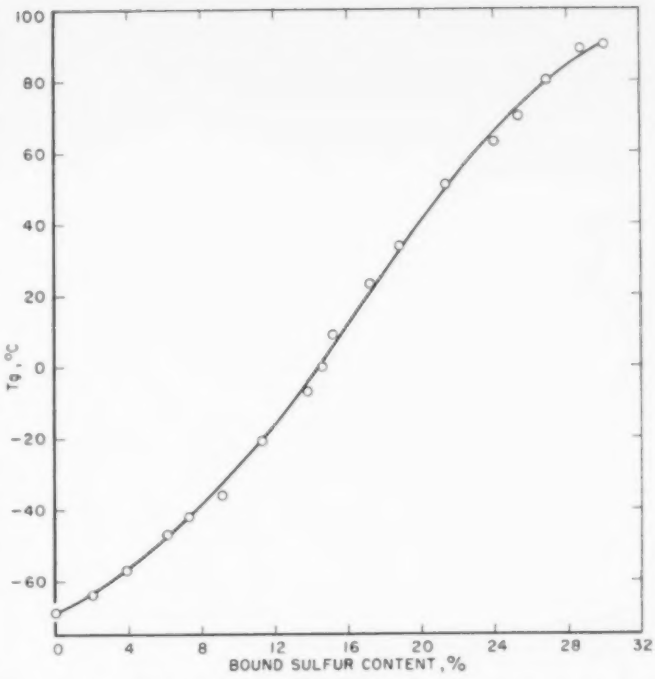

FIGURE 2. *Plot of glass temperature, T_g, as function of bound sulfur content for rubber-sulfur vulcanizates.*

TABLE 1. *Thermal expansion data and glass transition temperatures for natural rubber-sulfur vulcanizates*

Nominal sulfur content	Bound sulfur content	V_{25} Measured specific volume at 25° C	$(V_{25})_l$ Specific volume [a] in liquid state at 25° C	T_g Glass transition temperature	α_l Slope volume-temperature curve above T_g	α_g Slope volume-temperature curve immediately below T_g
%	%	cm^3/g	cm^3/g	°C	cm^3/g °C	cm^3/g °C
0	0.0	1.095	1.095	−69	775×10^{-6}	223×10^{-6}
2	2.0	1.078	1.078	−64	762	219
4	3.9	1.059	1.060	−57	748	202
6	6.1	1.040	1.040	−47	727	211
8	7.3	1.021	1.025	−42	688	188
10	9.1	1.005	1.010	−36	708	197
12	11.3	0.985	0.988	−21	638	198
14	13.8	.965	.966	−7	645	188
15	14.6	.958	.960	0	616	165
16	15.2	.948	.951	+9	599	212
18	17.2	.933	.935	23	581	199
20	18.8	.919	.920	34	566	188
22	21.3	.906	.900	51	527	201
24	24.0	.894	.881	63	518	210
25	25.3	.884	.873	70	491	208
28	26.9	.872	.861	80	475	212
30	28.7	.861	.846	89	485	202
32	30.0	.850	.841	90	471	178

[a] The specific volumes are corrected for the amount of free sulfur present.

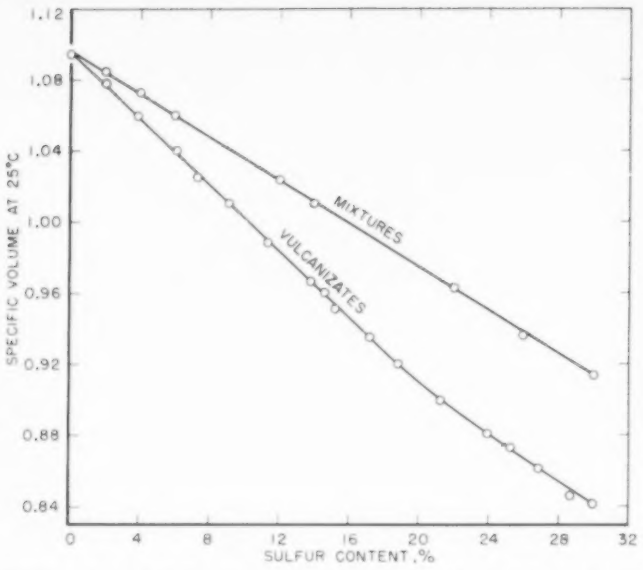

FIGURE 3. *Plot of specific volume in liquid state at reference temperature (25° C) against percent sulfur.*

Upper curve for mixture, lower curve for vulcanizate.

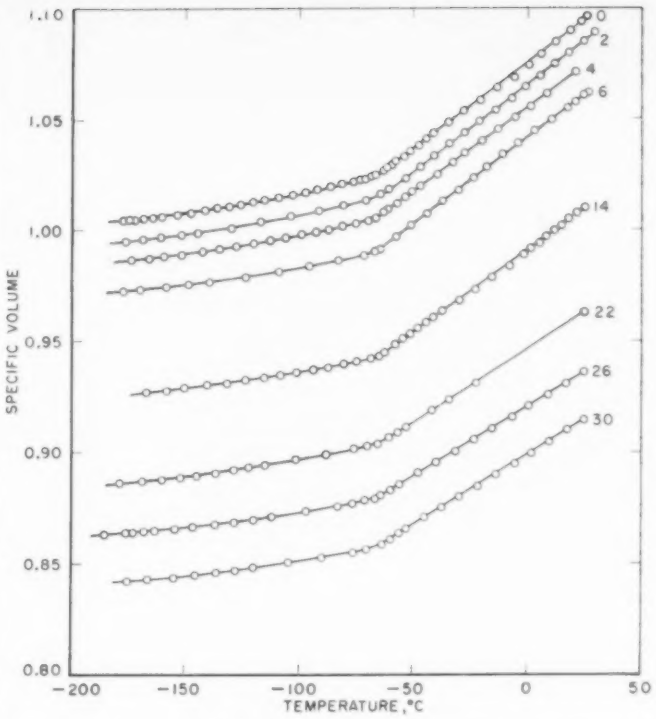

FIGURE 4. *Plot of specific volume as function of temperature for the rubber-sulfur mixtures.*

Number on right indicates percent sulfur.

less. If actual specific volumes had been plotted, this change in slope would have been even larger [8] because of the fact that at compositions of 19 percent or more sulfur the glass transition is above 25° C. In addition to the decrease in specific volume that is observed, there is also a significant continuous decrease in the volume-temperature coefficient above T_g, while a definite but smaller decrease occurs in the linear portion below T_g. The appropriate values of the volume-temperature coefficients are also given in table 1.

The volume-temperature relations for some typical natural rubber-sulfur mixtures, as contrasted to the chemically combined systems, are illustrated in figure 4. For each of the mixtures the data can again be well represented by a straight line in the liquid region and by a curved line in the glassy state. The glass temperatures, as determined from the data of figure 4, are remarkably constant and can be assigned a value of $-68°$ C $\pm 1°$ for all the mixtures. The dependence of the specific volume of the mixtures at 25° C on the sulfur content is also shown in figure 3; the data are well represented by a straight line. The values of the specific volume observed and those calculated by the additive mixing law agree very well and indicate that no net change in volume occurs on mixing. A similar observation was made some years ago by McPherson [8]. The pertinent physical constants for these mixtures are tabulated in table 2.

4. Discussion

The very large changes in the glass temperature of natural rubber that are induced by reaction with sulfur must be caused by the alteration of the liquid state structure. These changes in structure occur as a consequence of the chemical processes that have taken place. The natural rubber-sulfur reaction, though well known and intensively studied, is quite complex. There are wide areas of disagreement among various investigators as to the mechanism of the reaction and the resulting structures that are formed [15, 16]. It is clear, however, that a portion of the combined sulfur is utilized to form intermolecular crosslinks. The complexity of the chemical process precludes at present the possibility of ascribing the changes in T_g to specific chemical alteration, and somewhat more general considerations must be given to explain the drastic changes in the physical and mechanical properties that occur.

The variation of the glass temperature in other polymeric systems with the systematic alteration of structure or the composition has been satisfactorily

TABLE 2. *Thermal expansion data and glass transition temperatures for natural rubber-sulfur mixtures*

Nominal sulfur content	v_{25} Specific volume at 25° C	T_g Glass transition temperature	α_l Slope volume-temperature curve above T_g	α_g Slope volume-temperature curve immediately below T_g
$c_{\%}$	cm^3/g	° C	cm^3/g ° C	cm^3/g ° C
0	1.095	−69	775×10^{-6}	223×10^{-6}
2	1.085	−68	789	224
4	1.073	−68	756	196
6	1.060	−68	783	181
12	1.024	−67	553	198
14	1.010	−67	739	180
22	0.963	−67	651	180
26	.936	−68	619	168
30	.914	−68	630	157

explained on the basis of free volume considerations [3–7]. The problems treated, using this concept, have been those where the free volume itself need not be specified but the changes in the free volume, as manifested by the changes in the specific volume, are determined, and the change in T_g relative to that for a reference polymer can be calculated. This procedure is limited to cases where the changes that are occurring do not drastically alter the chemical or molecular structure of the polymer and has been successful in treating the molecular weight dependence of T_g [3], the effect of crosslinking [4], dilution with low-molecular-weight materials [5], copolymerization [5, 6], and the effect of increasing the number of groups in a polymer side chain [7]. It is of interest to apply the aforementioned ideas to vulcanizates of rubber-sulfur.

In utilizing this method the specific volume in the liquid state is assumed to consist of two parts; that volume which would be occupied by a closely packed liquid structure and the remaining volume which is termed the free volume. The net change in the specific volume of a given system, when subject to an external change, may reflect changes in the occupied volume, in the free volume, or in both. One consequence of the reaction of natural rubber with sulfur is that at a reference temperature in the liquid state the specific volume is reduced. Following procedures used in describing T_g for the poly(n-alkyl methacrylate) series of polymers, a certain fraction f of this volume change is attributed to a decrease in the free volume of the system, so that the relative change in free volume that occurs at temperature T can be expressed as

$$\phi^s(T)=\phi^0(T)-f[\overline{v}^0(T)-\overline{v}^s(T)] \qquad (3)$$

where $\phi^s(T)$ and $\phi^0(T)$ are the specific free volumes of the vulcanizate and pure rubber, respectively, and $\overline{v}^s(T)$ and $\overline{v}^0(T)$ are the corresponding values of the specific volumes at a temperature T in the liquid state. It is further assumed that the free volume varies linearly with temperature so that

$$\phi(T)=\phi_g+\Delta\alpha(T-T_g) \qquad (4)$$

where ϕ_g is the free volume at the glass temperature T_g, and $\Delta\alpha$ represents the rate of change of the free volume with temperature. By writing equation (4) for the vulcanizate and for pure rubber at a temperature T_R and substituting these results in equation (3), the following expression is obtained relating the glass temperature of the vulcanizate T_g^s to that of the pure polymer and to the volumes of the system:

$$T_g^s=T_R-(\Delta\alpha^0/\Delta\alpha^s)(T_R-T_g^0)+(f/\Delta\alpha^s)[\overline{v}^0(T)_R)-\overline{v}^s(T_R)]+(\phi_g{}^s-\phi_g{}^0)/\Delta\alpha^s \qquad (5)$$

where T_R is a reference temperature taken to be 298° K and the superscript ^{0} refers to pure rubber while the superscript ^{s} refers to the vulcanizate.

In order for equation (5) to be converted into a form that can be useful in interpreting the experimental results, it is necessary that the appropriate criterion for glass formation be specified. The simplest condition to take is that glass formation represents a state of isofree volume. This criterion was originally applied by Fox and Flory [3] in explaining the effect of molecular weight on the glass temperature of polystyrene and has been applied in explaining the effect of composition in copolymers and polymer-diluent mixtures and the effect of structural changes on the glass temperature of the poly(alkyl methacrylates). When the aforementioned criterion is applied, equation (5) simplifies to

$$T_g^s=298-94\Delta\alpha^0/\Delta\alpha^s+f/\Delta\alpha^s[\overline{v}^0(298)-\overline{v}^s(298)] \qquad (6)$$

It has been suggested [17, 18] that the condition $\phi_g/\overline{v}_g$ is a constant at T_g is a more satisfactory specification of glass formation. When this condition is introduced into equation (5) an additional term results in equation (6). However, it has been found that this slight correction does not sensibly alter the results [7].

Utilizing equation (6), values of f for each of the vulcanizates can be computed by using smoothed data derived from table 1 and assuming that the volume-temperature coefficient for the free volume can be identified with the difference in the corresponding coefficients in the liquid and glassy state. The quantities used in the calculation and the resulting values of f that are computed from equation (6) are given in table 3. It can be seen from these results that a reasonable value for the magnitude of the quantity f is obtained; it being less than unity and comparable to that obtained for other systems. As contrasted to the results for other systems, however, these deduced values of f

TABLE 3. *Calculation of* f, *the fraction of the specific volume change upon vulcanization which occurs in the free volume* [a]

Bound sulfur content	$\Delta\alpha^s$	$\overline{v}^0(298)-\overline{v}^s(298)$	f
%	$cm^3/g\ °K$	cm^3/g	
0.0	5.57×10^{-4}	0.000	
2.0	5.48	.017	0.226
3.9	5.38	.035	.230
6.1	5.22	.056	.261
7.3	5.12	.068	.263
9.1	4.93	.085	.261
11.3	4.68	.107	.289
13.8	4.38	.129	.299
14.6	4.27	.137	.305
15.2	4.19	.143	.319
17.2	3.91	.160	.322
18.8	3.68	.175	.318
21.3	3.35	.195	.313
24.0	3.03	.214	.296
25.3	2.90	.223	.294
26.9	2.81	.234	.289
28.7	2.72	.246	.283
30.0	2.72	.254	.274

[a] The values in the second and third columns are taken from smoothed curves, $\Delta\alpha^s=5.57\times10^{-4}$.

remain only approximately constant with increasing amounts of bound sulfur. They gradually increase from a value of 0.23 at 2 percent combined sulfur to a maximum value of 0.32 at 17 percent sulfur and then slowly decrease once again. Though the deviation of each value of f from the mean is not very large, the lack of constancy in this quantity is such that using the mean value of f in equation (6) does not adequately represent the data of figure 2.

From free volume considerations it would be expected that the glass transition temperature for the rubber-sulfur vulcanizates should increase as the amount of combined sulfur increases since a concomitant decrease in specific volume occurs. Though this effect is observed, the simple relation that has been derived in equation (6), though known to be applicable to other systems [7], is only qualitatively correct for the system discussed in the present work. The reason for the lack of quantitative agreement in this instance, when compared to other systems, can be due to complications caused by structural alterations induced by the chemical processes. Even at the lower levels of bound sulfur only a portion of the sulfur is involved in intermolecular crosslinks, the fate of the remainder of the sulfur being still a matter of argument [16]. The structure of the compounds containing the higher amounts of bound sulfur is still obscure. With the distinct possibility existing of major structural changes on reaction with sulfur it is not surprising that the relatively simple consideration set forth above yields only qualitative agreement with experiment. It must also be remembered that 32 percent bound sulfur corresponds to one sulfur atom bound per isoprene unit. On this basis a relatively large amount of sulfur is incorporated into the compounds and could thus be treated as a second component, similar to a copolymeric ingredient or low molecular weight diluent. Although, in a formal fashion, the problem can be treated from this point of view by methods previously described [5, 6], several arbitrarily selected parameters are required which can not be evaluated independently. Thus, the physical significance of the results is open to question.

On the other hand, in the case of the natural rubber-sulfur mixtures the concepts outlined above appear to apply very well. In this instance there is no net change in the specific volume of the system on mixing over the complete composition range. Thus the free volume available to the polymer is neither increased nor decreased and consequently T_g remains invariant with composition.

5. References

[1] R. F. Boyer and R. S. Spencer, Advances in colloid science, edited by H. Mark and G. S. Whitby, vol. 2, p. 1 (Interscience Publishers, New York, N.Y., 1946).
[2] W. Kauzman, Chem. Rev. **43,** 219 (1948).
[3] T. G. Fox and P. J. Flory, J. Appl. Phys. **21,** 581 (1950).
[4] S. Loshaek, J. Polymer Sci. **15,** 391 (1955).
[5] T. G. Fox, Bull. Am. Phys. Soc. [2] **1,** 123 (1956).
[6] L. Mandelkern, G. M. Martin, and F. A. Quinn, Jr., J. Research NBS **58,** 137 (1957) RP2745.
[7] S. S. Rogers and L. Mandelkern, J. Phys. Chem. **61,** 985 (1957).
[8] A. T. McPherson, BS Sci. Paper **22,** 383 (1927).
[9] A. H. Scott, J. Research NBS **14,** 99 (1935) RP760; Rubber Chem. Tech. **8,** 401 (1935).
[10] R. N. Work, J. Research NBS **47,** 80 (1951) RP2230.
[11] G. E. Merritt, BS J. Research **10,** 59 (1933) RP515.
[12] G. M. Martin, S. S. Rogers, and L. Mandelkern, J. Polymer Sci. **20,** 579 (1956).
[13] L. A. Wood, N. Bekkedal, and F. L. Roth, J. Research NBS **29,** 391 (1942) RP1507.
[14] K. Schmieder and K. Wolf, Kolloid-Z. **134,** 149 (1953).
[15] E. H. Farmer, Advances in colloid science, edited by H. Mark and G. S. Whitby, Vol. 2, p. 299 (Interscience Publishing Co., New York, N.Y., 1946).
[16] D. Craig, Rubber Chem. Tech. **30,** 1291 (1957).
[17] M. L. Williams, R. F. Landel, and J. D. Ferry, J. Am. Chem. Soc. **77,** 3701 (1955).
[18] F. Bueche, J. Chem. Phys. **24,** 418 (1956).

WASHINGTON, November 24, 1958.

Journal of Research of the National Bureau of Standards Vol. 62, No. 4, April 1959 Research Paper 2945

Elastic Deformations in Strips With Holes Loaded Through Pins

Michael Chi and L. K. Irwin

Bickley's solution for the generalized plane stress in a plate loaded through a pin is extended to give the deformation at any point in a plate loaded through one or two pins which are on the same load line. Analytical expressions are derived that are known to apply to a finite strip with a width $\geq 14a$ and distance between holes $\geq 8a$, where a is the radius of the hole. Numerical examples are developed and presented in the form of graphs for typical cases.

1. Nomenclature

a = radius of the hole
K_n = constant coefficients, e.g., $K_0=\frac{1}{2}$, $K_1=-\frac{1}{12}$, $K_2=0$, $K_3=\frac{1}{120}$, $K_4=0$, etc.
E = Young's modulus of elasticity
G = modulus of rigidity, $\frac{E}{2(1+\mu)}$
n = positive integers from 0 to ∞ in an infinite series whose general term is $f(n)$
n_o = a positive integer arbitrarily chosen to designate the first term of a partial series
p = maximum intensity of the pressure from the pin on the hole
P = total force exerted by pin on the boundary of hole
r,θ = polar coordinates
s = partial sum of a series
u = displacement in radial direction
v = displacement in tangential direction
w_x = displacement in longitudinal direction
w_y = displacement in transverse direction
$\gamma_{r\theta}$ = shearing strain
ϵ_r = strain in radial direction
ϵ_θ = strain in tangential direction
μ = Poisson's ratio
μ' = modified Poisson's ratio in a generalized plane stress problem, $\mu/(1+\mu)$
σ_r = normal stress in radial direction
σ_θ = normal stress in tangential direction
$\tau_{r\theta}$ = shearing stress

2. Introduction

The loads applied to a plate can be transmitted to other plates through joints which are made with fasteners in holes. The loads produce shearing stresses in the fasteners which, in turn, produce compressive or "bearing" forces on the boundaries of the holes. The elastic stresses in the plate produced by the boundary force on a hole, if solved, can be used directly for the determination of the elastic deformations. These deformations are of primary importance in evaluating the suitability of different combinations of materials and fasteners for aeronautical structures.

This method cannot be applied to a strip of arbitrary dimensions loaded by pins because the general solution for the elastic stresses in this case has not been found. However, the problem of the elastic stresses in an infinite plate loaded by one rigid pin was solved by Bickley [1] [1] and the problem of a plate with a circular hole at its middle subjected to uniform unidirectional tension was solved by Kirsch [2]. The stresses given by the solutions contained in these papers are combined by superposition to obtain the stresses for the problem considered here. With the aid of these stresses, the deformations of finite strips loaded through one or two holes located on the load line are calculated.

3. Theory

Bickley's solution for the general plane stress function ϕ for an infinite plate loaded by one solid pin is:

$$\phi=a^2\left[A_0\log_e\frac{r}{a}+B_0\theta+A_1\left\{\frac{r}{a}\theta\sin\theta-\frac{1-\mu}{2}\frac{r}{a}\left(\log_e\frac{r}{a}\right)\cos\theta\right\}\right.$$
$$+B_1\left\{\frac{r}{a}\theta\cos\theta+\frac{1-\mu}{2}\frac{r}{a}\left(\log_e\frac{r}{a}\right)\sin\theta\right\}+C_1\frac{a}{r}\cos\theta+D_1\frac{a}{r}\sin\theta$$
$$\left.+\sum_2^\infty\{a^{m-2}r^{-m+2}(A_m\cos m\theta+B_m\sin m\theta)+a^m r^{-m}(C_m\cos m\theta+D_m\sin m\theta)\}\right] \quad (1)$$

where A_m, B_m, C_m and D_m are coefficients.

[1] Figures in brackets indicate the literature references at the end of this paper

The above expression satisfies the biharmonic equation based on compatibility considerations [3, p. 54],

$$\left(\frac{\partial^2}{\partial r^2}+\frac{1}{r}\frac{\partial}{\partial r}+\frac{1}{r^2}\frac{\partial^2}{\partial \theta^2}\right)\left(\frac{\partial^2\phi}{\partial r^2}+\frac{1}{r}\frac{\partial\phi}{\partial r}+\frac{1}{r^2}\frac{\partial^2\phi}{\partial\theta^2}\right)=0,$$

and has single-valued deformations and stresses.

The stresses in polar coordinates in terms of the stress function ϕ which satisfy the equations of equilibrium are [3, p. 52]:

$$\left.\begin{aligned}\sigma_r&=\frac{1}{r}\frac{\partial\phi}{\partial r}+\frac{1}{r^2}\frac{\partial^2\phi}{\partial\theta^2}\\ \sigma_\theta&=\frac{\partial^2\phi}{\partial r^2}\\ \tau_{r\theta}&=-\frac{\partial}{\partial r}\left(\frac{1}{r}\frac{\partial\phi}{\partial\theta}\right).\end{aligned}\right\}\qquad(2)$$

The distribution of the forces due to the pin load is customarily assumed to vary as a cosine function over half the boundary of the hole [1; also 4, p. 123]. This has been confirmed by experiment [1]. Since cosine functions are even functions, we can represent the distribution of the boundary forces on the edge of the hole due to the pin by the Fourier cosine series:

$$f(\theta)=\frac{a_0}{2}+\sum_1^\infty a_m\cos\ m\theta.\qquad(3)$$

The coefficients are determined by a known distribution of boundary forces,

$$f(\theta)=p\cos\theta,-\frac{\pi}{2}\leq\theta\leq\frac{\pi}{2},$$

$$=0\qquad\text{elsewhere.}$$

Since the stresses at the edge of the hole must be equal to the boundary forces, due to the pin, the coefficients in eq (1) may be determined by substituting eq (1) in eq (2), performing the indicated partial differentiations, and then equating the resulting stresses at the edge of the hole to the forces, eq (3). If the distribution, $f(\theta)$, is assumed acting, the stresses, eq (2), become

$$\left.\begin{aligned}\sigma_r&=-p\left[\frac{1}{\pi}\left(\frac{a}{r}\right)^2+\frac{3+\mu'}{8}\frac{a}{r}\cos\theta-\frac{1-\mu'}{8}\left(\frac{a}{r}\right)^3\cos\theta\right.\\ &\qquad\left.+\sum_{2,4,6,\ldots}^{\infty}\frac{1}{2\pi}\left\{\frac{\sin\frac{m+1}{2}\pi}{m+1}+\frac{\sin\frac{m-1}{2}\pi}{m-1}\right\}\left(\frac{a}{r}\right)^m\cos\ m\theta\left\{2+m\left(1-\frac{a^2}{r^2}\right)\right\}\right],\\ \sigma_\theta&=p\left[\frac{1}{\pi}\left(\frac{a}{r}\right)^2+\frac{1-\mu'}{8}\frac{a}{r}\cos\theta+\frac{1-\mu'}{8}\left(\frac{a}{r}\right)^3\cos\theta\right.\\ &\qquad\left.+\sum_{2,4,6,\ldots}^{\infty}\frac{1}{2\pi}\left\{\frac{\sin\frac{m+1}{2}\pi}{m+1}+\frac{\sin\frac{m-1}{2}\pi}{m-1}\right\}\left(\frac{a}{r}\right)^m\cos\ m\theta\left\{-2+m\left(1-\frac{a^2}{r^2}\right)\right\}\right],\\ \tau_{r\theta}&=p\left[\frac{(1-\mu')}{8}\frac{a}{r}\sin\theta-\frac{1-\mu'}{8}\left(\frac{a}{r}\right)^3\cos\theta\right.\\ &\qquad\left.-\sum_{2,4,6,\ldots}^{\infty}\frac{1}{2\pi}\left\{\frac{\sin\frac{m+1}{2}\pi}{m+1}+\frac{\sin\frac{m-1}{2}\pi}{m-1}\right\}\left(\frac{a}{r}\right)^m\sin\ m\theta\left\{m\left(1-\frac{a^2}{r^2}\right)\right\}\right].\end{aligned}\right\}\qquad(4)$$

Since eq (1) was derived using plane strain theory, the above equations were made applicable for a generalized plane stress solution by replacing Poisson's ratio, μ, with μ' which is equal to $\mu/(1+\mu)$ [5].

In polar coordinates, the stress-strain-deformation relationships are

$$\left.\begin{aligned}\frac{\partial u}{\partial r}&=\epsilon_r=\frac{1}{E}(\sigma_r-\mu'\sigma_\theta)\\ \frac{\partial v}{\partial\theta}+u&=r\epsilon_\theta=\frac{r}{E}(\sigma_\theta-\mu'\sigma_r)\\ \frac{1}{r}\frac{\partial u}{\partial\theta}+\frac{\partial v}{\partial r}-\frac{v}{r}&=\gamma_{r\theta}=\frac{1}{G}\tau_{r\theta}.\end{aligned}\right\}\qquad(5)$$

Substituting the first and second expressions of (4) into the first part of eq (5) and integrating,

$$u=\int \epsilon_r dr\Big]_{\theta=\text{const}}=\frac{1}{E}\int(\sigma_r-\mu'\sigma_\theta)\,dr$$

similarly,

$$v=\frac{1}{E}\int r\,(\sigma_\theta-\mu'\sigma_r)\,d\theta-\frac{1}{E}\int(\sigma_r-\mu'\sigma_\theta)\,dr \qquad (6)$$

By substituting (6) into the last of eq (5), it can be shown that the constants of integration are rigid body displacements [3, p. 189] and therefore may be set equal to zero for the purposes of this investigation.

Thus far, only the infinite plate with the load applied through a pin at the middle and supported at infinity [6] as shown in figure 1(a) has been considered. The complete solution of the problem, figure 1(c), is obtained by superposing the solutions of two subproblems, figures 1(a) and 1(b). The problem of a plate with a circular hole at its middle and subject to a uniform unidirectional tension, figure 1(b), is the well known Kirsch's problem which can be found in standard texts [3, p. 195].

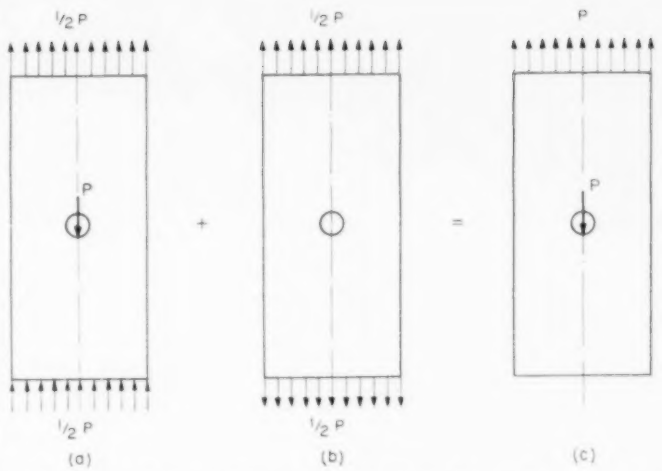

FIGURE 1. *Superposition of subproblems* (a) *and* (b) *to solve problem* (c).

Sketches represent infinite plates.

Combining these two solutions, the equations for radial and tangential displacements are, respectively,

$$\left.\begin{aligned}
u=&\frac{pa}{E}\left[\frac{1+\mu'}{\pi}\frac{a}{r}+\frac{3+2\mu'-(\mu')^2}{8}\left(\log_e\frac{a}{r}\right)\cos\theta+\frac{1-(\mu')^2}{16}\frac{a^2}{r^2}\cos\theta\right.\\
&+\sum_{2,4,6,\ldots}^{\infty}\frac{1}{\pi}\left(\frac{a}{r}\right)^{m-1}\left\{\frac{\sin\frac{m-1}{2}\pi}{m-1}+\frac{\sin\frac{m+1}{2}\pi}{m+1}\right\}\left\{\frac{m}{2}+1+\left(\frac{m}{2}-1\right)\mu'-\frac{m}{2}(1+\mu')\frac{a^2}{r^2}\right\}\cos m\theta\\
&\left.+\frac{\pi(1-\mu')}{128}\frac{r}{a}+\frac{\pi(1+\mu')}{128}\frac{a}{r}+\left\{\frac{\pi}{32}\frac{a}{r}+\frac{\pi(1+\mu')}{128}\frac{r}{a}-\frac{\pi}{128}(1+\mu')\frac{a^3}{r^3}\right\}\cos 2\theta\right]\\
v=&\frac{pa}{E}\left[\frac{1+2\mu'+(\mu')^2}{8}\sin\theta-\frac{3+2\mu'-(\mu')^2}{8}\left(\log_e\frac{a}{r}\right)\sin\theta+\frac{1-(\mu')^2}{16}\frac{a^2}{r^2}\sin\theta\right.\\
&+\sum_{2,4,6,\ldots}^{\infty}\frac{1}{\pi}\left(\frac{a}{r}\right)^{m-1}\left\{\frac{\sin\frac{m-1}{2}\pi}{m-1}+\frac{\sin\frac{m+1}{2}\pi}{m+1}\right\}\left\{\frac{-2+\frac{m}{2}(1+\mu')}{m-1}-\frac{\frac{m}{2}(1+\mu')}{m+1}\frac{a^2}{r^2}\right\}\sin m\theta\\
&\left.-\left\{\frac{\pi}{64}(1-\mu')\frac{a}{r}+\frac{\pi}{128}\frac{r}{a}(1+\mu')+\frac{\pi}{128}(1+\mu')\frac{a^3}{r^3}\right\}\sin 2\theta\right].
\end{aligned}\right\} \qquad (7)$$

μ' is taken as 0.25 for the purpose of this investigation.

The displacements in Cartesian coordinates can be evaluated from the radial and tangential displacements in polar cordinates by the following relationship [4, p. 18]:

$$\left.\begin{aligned}
w_x&=u\cos\theta-v\sin\theta\\
w_y&=u\sin\theta+v\cos\theta.
\end{aligned}\right\} \qquad (8)$$

Therefore, the displacements at any point in the infinite plate loaded through a pin can be found by substituting eq (7) into eq (8).

The displacements thus obtained are meaningless by themselves because they include an arbitrary amount of rigid body displacements. The displacements of interest are the relative displacements between the points in the plate and a chosen reference point. The point, $r=a$, $\theta=0$ is chosen as the

reference point. The displacement of any point is taken to be the difference between the displacement of that point as computed by eq (8) and the displacement of the reference point.

The rate of convergence of the series in the equations for the displacements, eq (7), varies with the distance of the point from the hole. The first five terms were sufficient to give an accuracy within one-half percent for the displacements at all points. The relative displacements are the differences between large numbers of the same order of magnitude. To insure sufficient accuracy in the final results, the displacements in eq (7) were therefore carried to nine significant figures. This involved, for example, the inclusion of 6 terms of the series for the points a distance 3 times the radius of the hole, $3a$, from the edge of the hole and 16 terms for points a distance $0.5a$ from the edge of the hole. For comparable accuracy at the edge of the hole, about 100 terms of the series would be required. To reduce the computational task, the following Euler-Maclaurin Formula for computing the partial sum of the series was employed.

$$s=\sum_{0}^{n_0-1} f(n) + \int_{n_0}^{n_0+1} f(n)dn + \sum_{m=0}^{\infty} K_m 2^m \frac{d^m}{dn^m} f(n) \Bigg]_{n_0+1}^{n_0}.$$

In this case, $f(n)=\frac{2}{\pi}\frac{4n+1-\mu'}{(4n^2-1)^2}$.

4. Finite Strip With One Hole

In a plate of finite width, a hole close to an edge of the plate may have considerable effect on the stress distribution in the plate. The case of a plate of finite width (strip) with a circular hole on the axis of a symmetry was solved by a method of successive approximations [7]. The method was later extended to the case in which the hole is loaded through a pin [8]. However, the strain expressions obtained by this method were not suitable for integrating to obtain the displacements.

For strips whose width is large compared with the diameter of the hole, ratio of diameter of hole to width of strip less than 0.15, the effects of the edges of the strip on the stresses around the hole can be neglected [9]. On this basis, the displacements of an infinite plate due to a load applied through a pin are assumed to be applicable to a finite strip without serious error. Figure 2 shows the relative displaces ments along the longitudinal centerline and the edgefor a strip with one pin. The diameter to width ratio is equal to 0.125.

5. Finite Strip With Two Holes

The stresses around a hole are influenced by the presence of adjacent holes. The method of successive approximations is again applicable to this case [10] but becomes much more complicated for the case of two or more holes with boundaries loaded through pins.

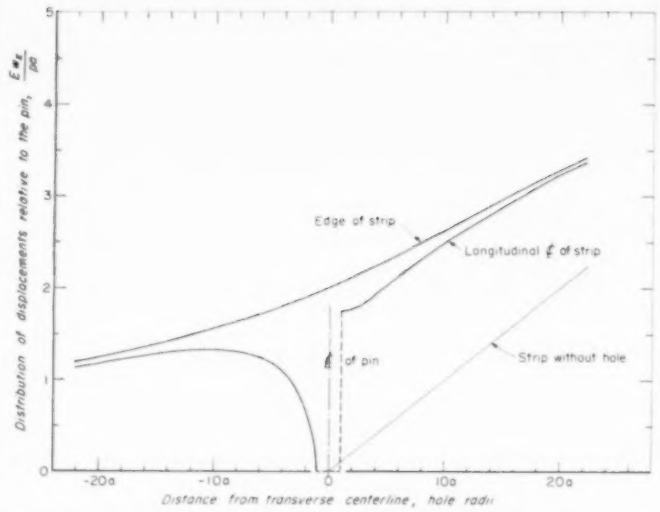

FIGURE 2. *Relative displacements along the longitudinal centerline and the edges for a strip with one pin.*

As previously mentioned, the effect of a hole in a plate is a local phenomenon, and the effects of adjacent holes on each other can be neglected [9] if they are sufficiently far apart; that is, if the center to center distance of the holes is four or more times the diameter of the larger hole. Thus for a spacing exceeding four hole diameters, the displacement of a point in a plate containing two holes loaded through pins can be taken equal to the sum of the displacements due to each hole taken separately.

The relative displacements along the longitudinal centerline and along the edges of a strip with two equidiameter holes located on the longitudinal centerline and loaded through pins are shown in figure 3. The holes are four diameters apart and the ratio of the diameter of the hole to the width of the strip equals 0.125.

6. Concluding Remarks

The analytical expressions and the computational methods presented here are applicable for determining the elastic deformations of finite strips loaded by pins when the effects of edges and interference between adjacent holes are negligible. Such strips have widths $\geq 14a$ and distances between holes $\geq 8a$. The examples for which deformations are shown in figures 2 and 3 correspond directly to single-shear test specimens widely used to evaluate the performance of joints. Further studies should be made to extend the range of these results.

This investigation was part of a project conducted under the sponsorship of the Bureau of Aeronautics. The authors wish to thank this agency for its support of this work.

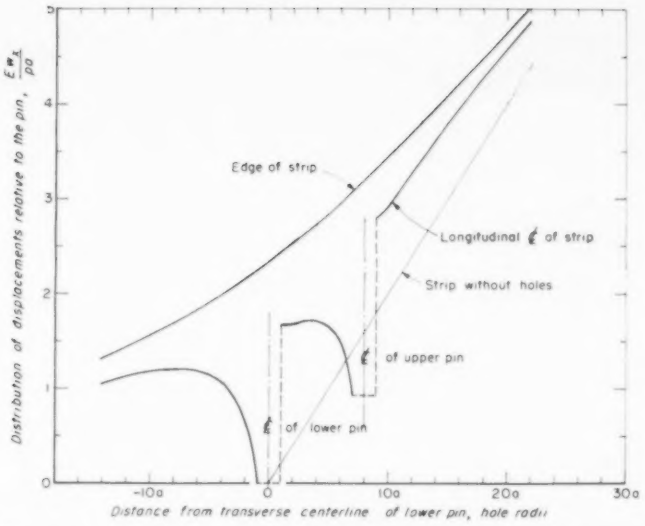

FIGURE 3. *Relative displacements along the longitudinal centerline and the edges for a strip with two pins.*

7. References

[1] W. G. Bickley, Phil. Trans. Roy. Soc. (London) [A **227,** 383 (1928).

[2] G. Kirsch, Z. Ver. deut. Ing. **42,** 797 (1898).

[3] C. T. Wang, Applied elasticity (McGraw-Hill Book Co., New York, N.Y., 1953).

[4] S. Timoshenko and J. N. Goodier, Theory of elasticity, 2d ed. (McGraw-Hill Book Co., New York, N.Y., 1951).

[5] A. E. H. Love, A treatise on the mathematical theory of elasticity, 4th ed., pp. 103, 138, and 208 (Dover Publications, New York, N.Y., 1944).

[6] R. C. J. Howland, Proc. Roy. Soc. (London) [A] **124,** 101 (1929).

[7] R. C. J. Howland, Phil. Trans. Roy. Soc. (London) [A] **229,** 49 (1930).

[8] R. C. J. Howland, Proceedings of the Third International Congress of Applied Mechanics, vol. II. 74 (1930).

[9] A. Atsumi, J. Appl. Mechanics **23,** 555 (1956).

[10] R. C. J. Howland, Proc. Roy. Soc. (London) [A] **148,** 471 (1935).

WASHINGTON, November 13, 1958.

Journal of Research of the National Bureau of Standards Vol. 62, No. 4, April 1959 Research Paper 2946

Absolute Light-Scattering Photometer: I. Design and Operation

Donald McIntyre and G. C. Doderer [1]

A new light-scattering photometer has been designed and built for determining the absolute scattering from polymer solutions. The instrument is also capable of performing as a research instrument for making measurements at very low and very high angles, and at very low and very high intensities of scattered light. The instrument scans the angular scattering either manually or automatically while measuring continuously the ratio of the scattered light to the incident light.

1. Introduction

The general need for accurate light-scattering measurements for the determination of molecular weights of high polymeric compounds is well known.[2] Some of the problems connected with these measurements and most of the work up until 2 years ago have been summarized in two publications.[3,4] The present work was done with the object of increasing the accuracy of determining molecular weights of macromolecules rather than that of determining optical constants of materials.

The instrument described here was designed to attain an accuracy of 3 to 5 percent in the determination of molecular weights. An instrument that must be versatile enough to make molecular weight measurements in any research problem and also make absolute scattering determinations imposes many compromises in design. For example, a closed-in system is much more convenient for general laboratory work, whereas an open system in a darkroom would be more suitable for absolute measurements. A compromise is to make a rather large working compartment in the instrument. Also, an absolute measurement would only have to be carried out at a few fixed angles so that considerably more rigidity and inflexibility could be built into an instrument to attain more accurate measurements. In contrast, a research instrument must be capable of scanning a large angular range with a measuring technique that is not unduly time consuming and fatiguing.

With these thoughts in mind an instrument was constructed with emphasis on providing (1) a variety of precise experimental setups involving different combinations of sources, lightbeams, filters, sample cells, and receiver arrangements; (2) a well-collimated beam of monochromatic light having uniform intensity and producing negligible stray light inside the instrument; (3) a sensitive and stable electronic detecting and recording system; and (4) a rugged mechanical design featuring easily adjusted components.

[1] Guest worker at the National Bureau of Standards from the Office of the Surgeon General, Department of the Army. Present address: General Electric Co., Louisville, Ky.

[2] H. P. Frank and H. Mark, J. Polymer Sci. **17**, 1 (1955).

[3] K. A. Stacey, Light Scattering in Physical Chemistry (Academic Press, New York, N.Y., 1956).

[4] M. M. Fishman, Light Scattering by Colloidal Systems, An Annotated Bibliography, Technical Service Laboratories, River Edge, N.J., 1957 (also additional annual supplements).

2. Apparatus

2.1. General Description

The over-all plan of the instrument is shown in figure 1. A transformer connected to a voltage regulator operates a mercury vapor lamp to produce a small intense source of light. The image of the source is then projected as a monochromatic beam of variable collimation that has well-defined dimensions at the center of the cell (C). From there the beam passes on to a light trap where it is absorbed.

A very small percentage of the projected beam is reflected by a cemented glass prism on to a monitoring photomultiplier tube (Mon PM). The measuring photomultiplier tube (Meas PM) is mounted on a T-beam connected to a goniometer so that it can be rotated to view the light scattered from the sample, which is mounted on a stationary pedestal at the center of rotation. Both phototubes are similar and operate from the same power supply controlled by a voltage regulator. The phototube outputs are amplified and fed to a ratio recorder

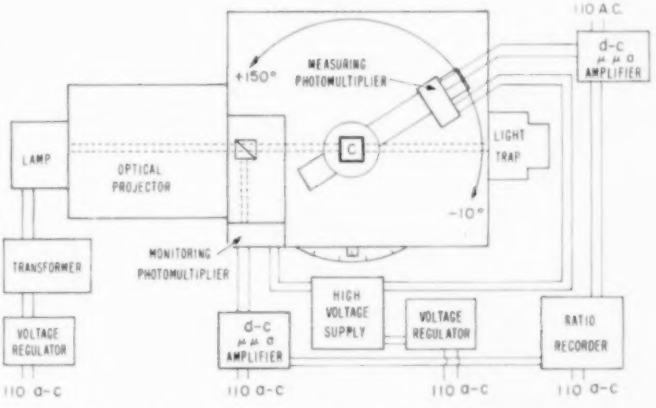

FIGURE 1. *Schematic diagram of photometer.*

which is essentially an automatic precision potentiometer operating a chart recorder. The recorder compares the voltage from the measuring circuit with the reference voltage from the monitoring circuit. Thus the amount of scattered light is measured relative to the incident beam and is recorded as a value which is independent of the absolute beam intensity.

Figure 2, an exterior view of the instrument, shows the source enclosure, optical projector, and goniometer housing mounted on a table and connected to the electronic control panel.

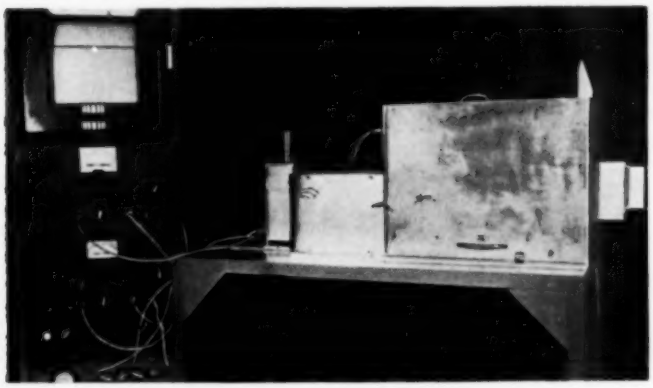

FIGURE 2. *Overall view of photometer.*

2.2. Optical System

The essential optical components are represented in figure 3. Two source lamps have been tested: an 85-w mercury vapor lamp, and a 250-w compact-source medium-pressure mercury vapor discharge lamp. The latter forms a discharge approximately 3.75 mm high by 1.5 mm wide between two chisel-edge electrodes. The chisel edges are alined in the direction of the optic axis so that the arc wanderings tend to occur along, rather than across the axis.

The source is located at the focal point of a plano-convex condensing lens L_1 of 84.5 mm focal length which receives light through a wide stop S_1 and a Corning 4600 special heat absorbing filter F_1. Essentially parallel light from lens L_1 passes through removable filters F_2 and F_3. F_2 represents three monochromatic filter combinations: (1) Corning glass filters 3389 and 5113 passing mercury blue light of wavelength 436 mμ; (2) Corning glass filters 3484, 5120, and 4303 passing mercury green light of wavelength 546 mμ; and (3) a multilayer interference filter also passing the mercury green line. F_3 represents 1 mm thick optical neutral glass filters, as do F_4 and F_5.

A second condensing lens L_2, similar to L_1, focuses an image of the source on aperture A_1 located at the focal point of lines L_3. The aperture A_1 is fitted into a milled slot and is removable so that variable degrees of beam collimation are obtainable. The largest aperture is 3.4 mm high by 1 mm wide so that it is smaller than the source image. Field stops which determine the size and shape of the projected beam may be inserted at position S_2 and adjusted axially so that the achromatic collimating lens L_3 of 98.6 mm focal length and 40-mm diameter focuses a sharp image of the field stop in the center of the sample cell, C. The beam can be shut off at the entrance to the main instrument housing by shutter Sh_1. The relative positions of the above components may be seen in figure 4. The remaining optical components inside the main housing are shown also in figure 5.

A 1-in. glass square consisting of two 45°–90° prisms cemented together with Canada balsam is indicated as G in figure 3. The cemented interface reflects a very small percentage of the incident light into the monitoring system. By choosing glass and cement of nearly the same refractive index, the same beam as that viewed by the measuring phototube may be monitored with minimum intensity loss and negligible polarization. Using barium crown glass of $n_d = 1.5415$, which was obtained from samples made at the NBS glass plant, and Canada balsam, which was reported to have an $n_d = 1.5446$, the measured reflectance from the surface was 10^{-5} of the incident green light. Thus the match of the refractive indices at this wavelength is closer than the above figures would indicate.

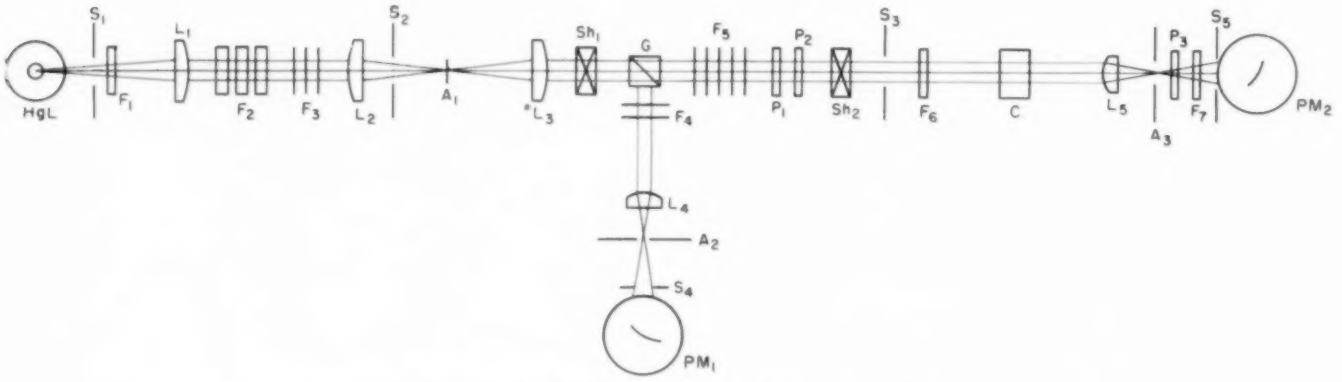

FIGURE 3. *Schematic diagram of the optical system.*

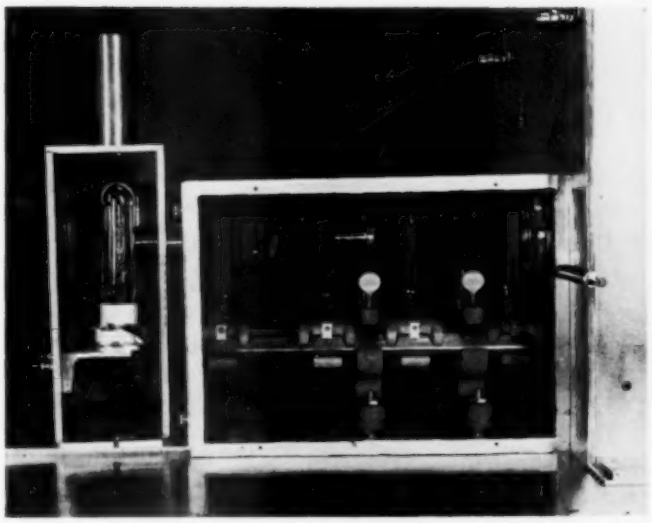

FIGURE 4. *Detailed view of the projector.*

FIGURE 5. *Detailed view of receivers and cell table.*

The main beam is attenuated by movable filters F_5 having transmittances of approximately 1/2, 1/3, 1/10, 1/40, and 1/4,500. P_1 and P_2 are Polaroid KN36 glass-laminated filters mounted with axes horizontal and vertical, respectively, and having maximum deviation of 4 min and maximum resolving power of 1 min. Shutter Sh_2 allows the measuring beam to be shut off without disrupting the monitoring system. S_3 is a baffle to eliminate stray light. In addition, removable baffles can be inserted into this nosepiece arrangement as beam dimensions are changed. Another tube can also be inserted on the cell table which is capable of accommodating two additional baffles. Thus there are four possible interchangeable baffles in addition to two shutter diaphragms, which are circular for eliminating stray light. A 4-mm-thick neutral glass filter F_6 of approximately 1/30,000 transmittance can be mounted on the end of the measuring phototube arm and subsequently brought into the lightbeam when the phototube is rotated into the beam. This is mounted as a milled slot so that other neutral filters can be inserted as they are needed. This arrangement is used only for automatic scanning of the entire angular scattering, and for special purposes of calibration.

The receiver optics consist of an achromatic lens L_5 of 40.5-mm focal length and 18.5-mm diameter, a small aperture A_3 mounted at the focal plane, and a stop S_5 which determines the area of lightbeam that is to be admitted to the phototube PM_2. There is a series of aperture stops, A_3, that can be easily and quickly inserted to define the angular acceptance of the receiver, just as there is a series of field stops, S_5, that can be inserted into the receiver in order to change the field of view consonant with the physical limitations of the phototube. The position of the whole receiver is adjustable so that the image of the field stop can be placed directly at the center of rotation. A Polaroid HN22 filter P_3 is mounted in a slide and can be adjusted to rotate 90° between the axes of the polarizers. A second slide F_7 may be used to hold a fluorescence filter. In addition, provision is made to insert a diffusor behind the field stop when necessary.

The monitoring optics consist of lens L_4, aperture A_2, field stop S_4, and phototube PM_1, similar to those in the measuring receiver just described. Attenuating filters F_4 having transmittances of approximately ⅛ and 1/56 are also placed before this receiver.

There are two interchangeable phototube housings on the measuring photo tube. Each of these housings can accommodate the receiver mount described, and can be placed into position without significant changes by means of milled slots. One housing contains a 1P21 photomultiplier which is used routinely, while the other housing contains an end-on photomultiplier, 5819, for special work. In addition, the latter housing can take a cassette which uses 1 by 3 in. photographic plates in place of the photomultiplier.

2.3. Electronic System

The sensitive and stable detecting-recording system is based upon the use of matched precision components in the monitoring and measuring circuits which operate the ratio recorder. Optionally, the recorder may be operated as a typical potentiometer recorder to indicate the output of either phototube separately. The receivers are closed desiccated metal housings containing RCA 1P21 multiplier phototubes. A power supply having 1-ma d-c output, stabilized to 0.5 percent and fed by a 0.250-Kva voltage stabilizer, is used for the high-voltage supply. When operated at 800 v d-c the phototube dark currents are about 3×10^{-10} amps. The monitor light beam may be adjusted to its maximum unfiltered intensity, which produces a total output of over 1×10^{-6} amps. Thus dark-current fluctuations have a negligible effect on the final monitor reference voltage. In

practice, a monitor output of about 1×10^{-8} amp has proven very satisfactory. The phototube outputs are amplified by two Leeds and Northrup 9836A stabilized d-c micromicroampere indicating amplifiers providing a full scale output of 10 mv over a range of 1×10^{-9} to 2×10^{-6} amp with an accuracy of ±0.5 percent of the range or 0.5×10^{-11} amp at the most sensitive region. The measuring circuit amplifier supplies voltage to the potentiometer of a Speedomax ratio recorder where it is compared with the monitor reference voltage to an accuracy of 0.3 percent of the range.

Thus fluctuations in source intensity affect both input voltages proportionately, and the final recorded value is independent of the absolute beam intensity. In operation, the measured values are corrected by subtracting a dark current reading with the shutter Sh_2 closed. This is done either arithmetically or by the use of a biasing voltage on the measuring phototube signal using a mercury cell.

The 85-w lamp operates from a transformer on 110 v a-c; whereas, the 250-w lamp operates from a ballast on a 220 v a-c line.

2.4. Mechanical Elements

The instrument was constructed as three independently adjustable assemblies; namely, the source, the optical projector, and a light-tight measuring compartment mounted on a heavy welded steel framework table top. All of these pieces were optically alined using the center of rotation of the measuring phototube and goniometer as a fiducial mark. Visual observations of the beam by means of targets placed in indexed positions along the rotating beam and center of rotation were used for the final alinement. Although the overall construction is sturdy to minimize possible vibration or movement, a wide range of adjustability is maintained. Thus the receiver apertures and field stops thread into place against positioning rings, and the mounts are positioned with the aid of pins.

The measuring phototube housing is mounted in machined ways on an aluminum beam of large T-cross section. With a narrow slit in front of the receiver lens, the entire housing may be moved across the lightbeam by a screw to determine the uniformity of the light flux. The aluminum beam is connected to a goniometer which is graduated in degrees from $-10°$ to $+150°$ with respect to the incident light. The assembly may be rotated manually as desired, or automatically in either direction by a reversible geared motor drive. A scanning rate of 40°/min was used to synchronize with the chart recorder speed of 2 in./min. Two electrical limit switches prevent mechanical damage due to overscanning and a third microswitch is operated by pins spaced 10° apart on the goniometer to activate a magnetic pen marker which produces a fiducial mark on the chart.

Sample cells and thermostats are positioned accurately on a stationary pedestal at the center of rotation by a three-point support system. The pedestal top has three ¼-in.-diam ball bearings on ⅜-in.-diam holes spaced 120° apart on a 3-in.-diam circle centered on the axis of rotation. Each cell assembly is cemented to a similarly drilled plate which automatically indexes on the pedestal with no undesirable mechanical tight fits or fastenings.

The light trap has two sections containing dark neutral filter glasses mounted at 45° to the incident beam. These filters at this angle of incidence absorb most of the light, reflecting only a few percent from their surfaces. In the large first section which absorbs low intensity scattered light surrounding the main beam, the filter surfaces reflect any light onto the black-painted trap walls where further reflection is negligible. The center of the first section is open and passes the main beam into the second section.

In this section the light undergoes two absorptions and 45° reflections by filter glass until it is finally directed to a black-painted portion of the trap not visible to the interior of the instrument compartment. The entire light trap is removable so that the interior may be viewed by a camera or telescope.

The photometer is also capable of operating at high temperatures since the cell table fixtures are located only by means of ball bearings which partially insulate the shaft below from the cell. Also the individual photometer housings are water cooled on the front plate to prevent any increase in the dark current by radiation from the sample.

3. Performance

3.1. Electronic

The 250-w lamp provides a light intensity approximately 11 times that of the 85-w lamp, but the arc is relatively unstable and would produce unacceptable errors in a single channel instrument, as is shown in the upper portion of the recorder trace in figure 6. The lower portion shows a trace under identical conditions, but using the monitored ratio-recording system. Here the trace variations are reduced to the small noise inherent in a high level d-c amplification system. From such a trace a constant average value is easily read.

In order to determine the response characteristics of the measuring system over a large range of intensities the transmittance of a neutral filter of approximately ½ transmittance was determined while reducing the lightbeam intensity with a neutral filter. In this work a large viewing field was used on the photomultiplier to eliminate the small inevitable local variations in a neutral filter. In changing the intensity by a factor of 1,000, the measured transmittance of the filter showed a maximum deviation of less than 1 percent with an average deviation of less than 0.5 percent. This is a severe test because in the very low intensity measurements the signal is much less than that from pure liquids and the ratio of dark current to total current becomes much larger.

Over several hours the system is very stable; however, the ratio of scattered light from an object will eventually change due to a small change of the temperature of the cemented prism. The small change

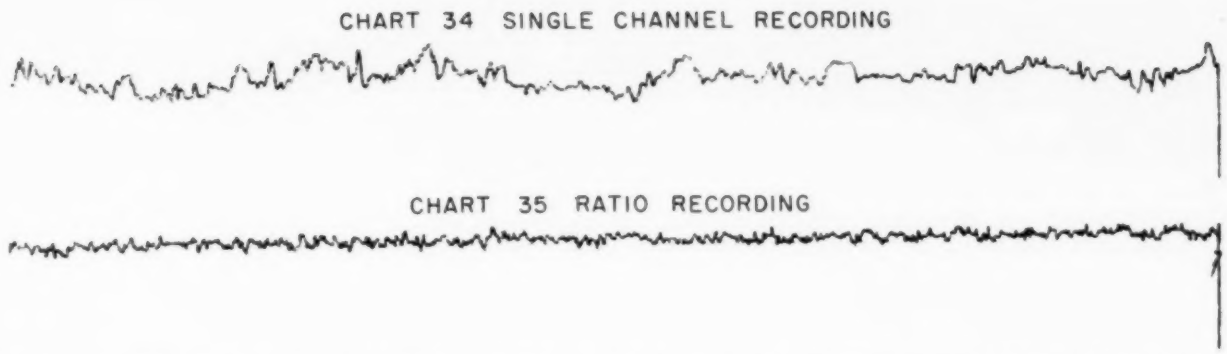

FIGURE 6. *Photometer trace of scattered light from a diffuser with (1) a single measuring photomultiplier, and (2) a ratio of two photomultiplier signals.*

in temperature in the prism can affect the percentage of reflected light so that the ratio can change. This is not critical since all measurements are made in the course of a few hours, and those kinetic measurements which last longer can easily be referred to the direct beam whether the scanning is manual or automatic.

3.2. Photometric

Stray light. In the early experiments observations were made to determine the existence of stray light which might be caused by some unforeseen peculiarity of the apparatus. Thus experiments were conducted with a nosepiece containing two stops which allowed the phototube to view a 6- by 10-mm field while accepting about 2.5°. The projected beam was about 10 mm wide and 12 mm high with a divergence of 0.5° in the horizontal direction and 1° in the vertical direction. Measurements were initially made shortly after changing stops with the box open. The photomultiplier current is measured as a function of viewing angle and of time after closing the top of the instrument. The data are listed in table 1. Below 12° the phototube receiver by visual observation appears to enter the edge of the large beam. The current in excess of the dark current can be attributed to stray light. From these results it appears that unless measures are taken to allow all of the dust to settle in the box the results in the forward direction will always contain a large amount of scattered light.

TABLE 1. *Photomultiplier currents at different angles and times*

Angle	Current in amperes		
	1 hr	1 day	2 days
150	22.7×10^{-11}		
120	17.6		
90	18.7		
60	28.4		
30	142.0	42×10^{-11}	22×10^{-11}
20		90	26
15			80
12			190
Dark current	22	20	16

The effects of adding diaphragms to eliminate stray light were also determined. There are four removable stray light baffles for a given beam size. They are located about 6 in. away from the projection lens and follow two circular iris diaphragms. They can be inserted about every 25 mm thereafter in the projected beam up to 100 mm from the center of rotation. They are in all cases slightly larger than the beam dimensions calculated for that location in the box. With the large beam (10 mm wide) no difference could be detected from 13° just outside of the large beam to 150° away from the direction of the beam when the stray light baffles were inserted or removed. Later a large cylindrical cell with plane entrance and exit windows and filled with a liquid whose refractive index was not too different from that of the glass was placed on the cell table and again there were no differences when the baffles were in or out of position or over the above angles. However, when the narrow beam (3 mm) was examined without a cell in place the stray light decreased by about 25 percent below 10° when appropriate baffles were introduced into the system.

In order to investigate further the effect of stray light the receiver was removed from the phototube housing so that the photomultiplier was receiving light from any angle that its photosensitive surface would allow. Again the addition of the baffles with the large beam while viewing from 45° to 150° showed no appreciable change in the response of the phototube. However, visual inspection after long dark adaptation indicated that a baffle in one of the middle positions did decrease some of the diffuse illumination in the photometer. From the results of all these experiments it is felt that this photometer can determine absolute amounts of scattered light from the usual organic liquids without any appreciable error from stray light.

Fluorescence, Polarization, and Monochromatic Filters. The directions of polarization were scribed on the Polaroid filters that were subsequently used for the polarizers. They were then mounted in the instrument by alining the inscribed marks with respect to the perpendicular and horizontal lines at the cell table. The analyzer was then set for extinction of the polarized beam. The percent

of transmission at extinction for the analyzer was 0.012 and 0.008 for blue light (436 mμ) in the horizontal and vertical direction, respectively, and 0.008 for 546-mμ light in both the horizontal and the vertical directions. The phototube was found to be equally sensitive to both horizontally and vertically prolonged light of 436 mμ wavelength, but was 0.5 percent more sensitive to horizontally prolonged light of 546 mμ wavelength.

Four filters for use with fluorescent solutions can be mounted in the barrel of the receiver. The No. 3384 Corning filter transmitted 9×10^{-4} percent of the 436-mμ light, and 88 percent of the 546-mμ light. The No. 2424 Corning filter transmitted 1.6×10^{-2} percent at 546 mμ and 7.8×10^{-6} at 436 mμ. These are simply cutoff filters to detect the amount of fluorescence. A set of monochromatic filters similar to those described below could also be used to allow light-scattering measurements to be made on fluorescent solutions.

The monochromatic filter combinations used for the incident beam were examined on a Beckman DK spectrophotometer and found to give less than 0.5 percent of the maximum intensity when measured at 200 A from 4358 and 5461 A. The transmission of the interference filter was about 2.5 times that of the glass filter.

Neutral Filters. Table 2 summarizes the results of many measurements made over a period of 9 months on the transmission values and their average deviations for the five neutral filters that are fixed in the instrument and moved reproducibly into position. The first four were always checked by the amplifier; whereas the very dense one was usually checked in comparison with another neutral filter and the amplifier. In some experiments a direct measurement of the dense filter transmission was made using the amplifier and gave good agreement with the comparison measurements even though the signal to noise ratio was extremely low. Table 3 gives the transmission results under changing experimental viewing conditions. Also table 2 indicates that the 1P21 and 5819 phototubes give the same transmission values. There is no question but that there is a slight nonuniformity of the transmittance over the total area of the neutral filter, as was seen in later experiments using a small slit to scan the filter; however, all ordinary measurements are carried out as above with fields of view of such dimensions that these small differences are integrated into a constant average value.

TABLE 2. *Transmittance of neutral filters for different phototubes at different wavelengths of light*

Filter	1P21 phototube		5819 phototube	
	436 mμ	546 mμ	546 mμ	436 mμ
1	0.495 ±0.6%	0.526 ±1.5%	0.532	0.502
2	.305 ±0.3%	.329 ±0.5%	.333	.305
3	.0792 ±0.5%	.0953 ±1%	.0971	.0794
4	.0190 ±0.5%	.0263 ±0.4%	.0264	.0191
5	6.64×10^{-3} ±0.2%	2.22×10^{-4} ±0.4%	2.26×10^{-4}	6.80×10^{-3}

TABLE 3. *Transmittance of neutral filters at 546 mμ for various size beams and different fields of view*

Filter	10-mm beam			3-mm beam
	5.5×9.9 mm	3.0×7.0 mm	5.04 mm diam	5.5×9.9 mm
1	0.526	0.527	0.522	0.552
2	.329	.329	.330	.323
3	.0964	.0970	.0964	.01016
4	.0263	.0262	.0264	.0260
5	2.22×10^{-4}	2.19×10^{-4}	2.20×10^{-4}	2.24×10^{-4}

Table 3 indicates no differences in the transmission values beyond experimental error when only the field of view is changed. However, special attention should be directed to the differences which appear when a beam which is smaller than the field of view of the photometer is used. These differing transmittances are no doubt due to the fact that a neutral filter with nonparallel faces or inexact perpendicular alinement can shift the lightbeam when placed in position. This shift then makes the entire lightbeam strike a different part of the photosensitive surface to give a slightly different signal. This causes no problem as long as the transmittance for such geometries is determined in the apparatus as it is used.

3.3. Optical

There are two optical systems to consider in the light-scattering photometer, namely, the projection system and the receiving system. In this instrument both systems are telecentric, that is, the aperture stop is located on the focal plane of the lens so that the principal ray in the projected beam is at all times parallel to the optic axis.[5] Figure 7 shows the diagram of the system for a lens L, of focal length f, an aperture stop S_2, and a field stop S_1. For the projection system the dimensions are: f=98.6 mm, r=318 mm, x=48.1 mm. From these dimensions the angular divergence of the beam, represented by one-half of the angle α in the diagram, and the magnification may be computed. It can be shown that with the dimensions in this instrument the angular divergence of the rays from the center

[5] L. Kushner, J. Opt. Soc. Am. **44**, 155 (1954).

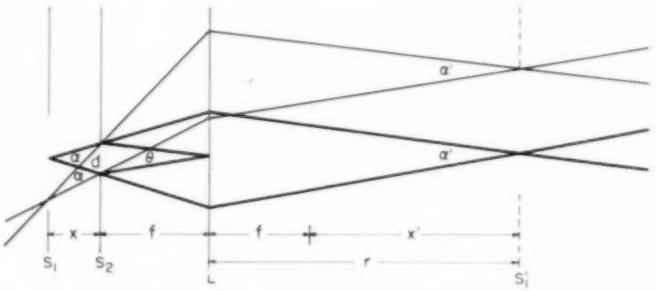

FIGURE 7. *A schematic representation of the telecentric system and the angles of beam projection or source acceptance.*

to the edge of the field stop differ by no more than 2 percent in the vertical direction with the largest aperture stop ever used, and by much less in the horizontal direction. The angular divergence of the most divergent projected beam is calculated to be 0.28° in the horizontal and 0.43° in the vertical direction, although for certain special measurements this beam was replaced by one having a 0.07° divergence in all directions. Although the divergence is difficult to measure exactly because of the indistinct image away from the field stop S_1' the divergence measured 250 cm away from S_1' gave agreement within a few percent of the calculated value.

In order to determine accurately the dimensions of the projected beam, measurements were made in three ways. Visual measurements were made with a telescope focused on a ruled glass scale located on the center of rotation. Then photographs were taken with a camera focused on the scale, and also on the centering fixture used for alining the instrument. The glass scale was particularly useful because it could be immersed in a solvent in a light-scattering cell to make certain of the unchanged magnification when the distance x in figure 7 was changed slightly to accommodate the decreased optical distance to the center of the cell. The results for three beams measured at the center of rotation are as follows: 9.20 $\pm$0.07 by 11.97 $\pm$0.10 mm, 3.09 $\pm$0.03 by 9.22$\times$0.07 mm, and 1.60 $\pm$0.03 mm diameter. The measured magnification of 2.06 is within 2 percent agreement of the calculated value.

The receiver system may also be represented by figure 7 and has the dimensions x=36.50, and r=78 to 117 mm. The achromatic lens used in the receiver, however, had its principal points determined on a nodal slide in the NBS Optics Division. The value for the equivalent focal length needed to calculate the angular acceptance of the system determined by S_1 and S_2 was 40.44 $\pm$0.10 mm for 575-mμ wavelength light. The aperture stop was located on the focal plane within $\pm$0.1 mm. The magnification of the field stop is about 1.11. The entire phototube housing can be moved so that the optical distance r may be kept constant by changing the geometrical distance when large size light-scattering cells are used and compared to quantities measured in air.

The beam uniformity has been tested in many ways. When the lamp is centered on the 1- by 3-mm aperture stop in the projector, the uniformity of the 9.2- by 12.0-mm beam as measured with a phototube having a 0.254-mm slit in front arranged to accept about 2.5° semicone angle, is constant within $\pm$0.5 percent over 95 percent of the beam. In this experiment the phototube housing is advanced across the beam by means of a screw with a pitch of 40 threads per inch. Evaluating more than this amount of the beam would require a smaller slit since the edge effects can be calculated to arise somewhere in this region. The same beam size at the center of rotation but having a smaller divergence gives the same results although the lamp is not as difficult to aline since less of the lamp area is required to fill the stop. As might be expected, the smaller size beams give the same uniformity.

Alinement of the receiver and beam direction is necessary for these measurements, and this can only be achieved by the use of mechanical fixtures followed by optical sighting methods. The end-on phototube does not appear as sensitive to extremely small angular deviations from parallelism as the 1P21.

The authors are indebted to P. Pfaff of the NBS Machine Shop for his many suggestions and excellent workmanship. They also thank E. Webb of the NBS Optical Shop for his construction of many of the optical components, and his cooperation in fitting and mounting many of the other items.

Journal of Research of the National Bureau of Standards Vol. 62, No. 4, April 1959 Research Paper 2947

Resolution of the Dissociation Constants of *d,l*-Malic Acid From 0° to 50° C [1]

Murray Eden [2] and Roger G. Bates

A method for the precise determination of the dissociation constants for the two overlapping dissociation steps of a weak dibasic acid from the same set of experimental data is described. The procedure, based on an earlier suggestion of Speakman (J. Chem. Soc. **1940,** 855), is applied to the resolution of the thermodynamic dissociation constants of *d,l*-malic acid at intervals of five degrees from 0° to 50° C. The constants were derived from measurements of the electromotive force of cells of the type

$$\mathrm{Pt;\ H_2(g),\ malate\ buffer\ solution,\ KCl}(m=0.008),\ \mathrm{AgCl;\ Ag.}$$

The 39 buffer solutions were prepared from potassium hydrogen malate and from mixtures of potassium hydrogen malate with perchloric acid or potassium hydroxide, and each contained potassium chloride. The first dissociation constant, K_1, is 3.48×10^{-4} at 25° C. It is given as a function of absolute temperature (T) by

$$-\log K_1=\frac{1358.85}{T}-5.1382+0.013550\,T.$$

The second constant, K_2, is 7.99×10^{-6} at 25° C. It is given by

$$-\log K_2=\frac{1658.53}{T}-6.2364+0.019353\,T.$$

The thermodynamic quantities ΔG°, ΔH°, ΔS°, and ΔC_p° related to each dissociation step were computed and compared with the corresponding constants for other acids closely related structurally to malic acid.

1. Introduction

The evaluation of the dissociation constants of a polybasic weak acid or polyacidic base is particularly difficult when the ratio of the constants for two successive dissociation steps is 100 or less. Even when the ratio of the first dissociation constant to the second is as high as 500, one of the constants cannot be evaluated without correcting for the effect of the other, inasmuch as some simultaneous dissociation occurs.

In view of these difficulties, the dissociation constants of only a few dibasic or polybasic acids with "overlapping" dissociation steps have been resolved in a precise way. Indeed, accurate values may be unobtainable by the usual experimental procedures. Consequently, little is known about the thermodynamic quantities associated with the separate overlapping ionization steps of acids of this type.

When the hydrogen ion concentration of a buffer solution is fixed by the interaction of a single acid or base with water, the dissociation constant can often be obtained with high accuracy from emf measurements by the method described by Roberts [1] [3] and by Harned and Ehlers [2]. This procedure has been so successful and has been used so widely that it may justifiably be termed the "conventional" emf method. Difficulties are usually encountered, however, when the dissociation constant of the acid or base exceeds 0.002 [3].

The cell most commonly used is a cell without transference, composed of a hydrogen electrode and a silver-silver chloride electrode. The same cell was utilized in the present study. It is represented by the following scheme

$$\mathrm{Pt;\ H_2(g),\ malate\ solution,\ KCl}(m=0.008),\ \mathrm{AgCl;\ Ag.} \qquad (1)$$

The reaction taking place when current is drawn from this cell is

$$\tfrac{1}{2}\,\mathrm{H_2}+\mathrm{AgCl}=\mathrm{Ag}+\mathrm{H^+}+\mathrm{Cl^-}.$$

Consequently, the emf E (corrected to 1 atm partial pressure of hydrogen) is related to the composition of the solution in the cell by

$$\frac{E-E^\circ}{2.3026RT/F}+\log m_{\mathrm{Cl}}=-\log\,(f_{\mathrm{H}}f_{\mathrm{Cl}}m_{\mathrm{H}}). \qquad (2)$$

In this equation, m represents molality (moles per kilogram of water), f is the activity coefficient on the molal scale, and E° is the standard potential (standard emf) of the cell. The values for the latter were derived from the work of Harned and

[1] Based on a dissertation presented by Murray Eden in partial fulfillment of the requirements for the Doctor of Philosophy degree at the University of Maryland, 1951. Presented before the Division of Physical Chemistry at the 134th Meeting of the American Chemical Society, Chicago, Ill., September 1958.

[2] Present address: Department of Health, Education, and Welfare, U.S. Public Health Service, National Institutes of Health, National Heart Institute, Bethesda 14, Md.

[3] Figures in brackets indicate the literature references at the end of this paper.

Ehlers [2, 4]. They have been tabulated in absolute volts in an earlier publication [5], together with values of the function $2.3026\,RT/F$ for temperatures from 0° to 60° C (absolute temperatures, T, from 273.16° to 333.16° K).

The expression relating the emf to the equilibrium constant, K, for the dissociation process,

$$HA^n + H_2O = H_3O^+ + A^{n-1}, \qquad (3)$$

where n represents the charge of the acid species HA, is derived by combining eq (2) with the mass-law expression for eq (3). The concentration of protons in dilute aqueous solutions is unknown, although it must be exceedingly small. However, as long as the activity of water remains substantially unity, the activity of protons will be proportional to the activity of the hydrates formed in reactions such as eq (3). Indeed, the hypothetical standard state of unit proton activity (to which $E°$ relates) corresponds by definition to an actual state in which hydrated protons or hydrogen ions are present at unit activity. Hence, m_H in eq (2) can be identified with $m_{H_3O^+}$ in the mass-law formulation of eq (3). These considerations are valid only as long as the activity of water remains substantially unity.

The indicated substitution gives

$$-\log K = -\log (f_H f_{Cl} m_H) - \log \frac{m_A}{m_{HA}} + \log \frac{f_{HA} f_{Cl}}{f_A} \qquad (4)$$

The activity-coefficient term at finite ionic strengths can be estimated by various means in order to facilitate the extrapolation of "apparent" values of $-\log K$ to infinite dilution, where the last term becomes zero and the true value of K is obtained. This method is quite elegant and completely satisfactory when the buffer pH is controlled by a single dissociation step of moderate strength and when the buffer solutions are stable in contact with the hydrogen and silver-silver chloride electrodes. It applies to polybasic acids and polyacidic bases if the ratios of the constants for successive dissociation steps are 10^3 or greater. The concentrations of the acid and its conjugate base are derived by correcting the stoichiometric molalities of these substances for hydrolysis and dissociation, that is, for reaction with the amphiprotic solvent.

The existence of a second acidic or basic group of a strength comparable with that under study complicates the determination considerably, for the concentration term of eq (4) can no longer be computed simply and accurately from stoichiometric concentrations [6, 7, 8, 9]. The quantity m_H in eq (2) is now a function simultaneously of more than one dissociation equilibrium, and the resolution of the individual constants may be a problem of considerable magnitude.

Nevertheless, it is sometimes possible to apply the "conventional" method successfully by choosing buffer ratios so that the hydrogen ion concentration is controlled almost exclusively by the dissociation step under study, a relatively small correction being made for the effect of the other. The procedure is an involved and laborious one. The dissociation constants of a number of weak dibasic acids have nonetheless been determined through variations of this general procedure [6, 10, 11, 12, 13]. In this way the dissociation constants of o-phthalic acid ($K_1/K_2 = 288$) have been resolved [12, 13] and the second dissociation constants of succinic acid ($K_1/K_2 = 27$) [14] and d-tartaric acid ($K_1/K_2 = 21$) [15] and the third dissociation constant of citric acid ($K_2/K_3 = 43$) [16] have been determined. In the last three instances a buffer ratio, m (neutral salt)/m (acid salt), of 3 was effective in keeping the hydrogen ion concentration low and in reducing the magnitude of the corrections for dissociation equilibria other than the one of primary concern.

Various attempts have been made to determine the overlapping dissociation constants simultaneously. In the method suggested by Speakman [17], the first and second dissociation constants for a weak dibasic acid are derived from a single set of observations. The experimental data are plotted in such a way that a straight line is obtained. The intercept is K_1K_2 and the slope determines the value of K_1. However, Speakman's method utilizes values of "hydrogen ion activity" ($\mathbf{a}_H$) from pH measurements and consequently does not furnish exact values of thermodynamic dissociation constants.

A method for determining the product of the overlapping ionization constants of a dibasic acid was proposed by Bates [18]. The complete resolution depends on an independent determination of one constant. The cell solutions contained known molalities of the acid salt of the weak dibasic acid and an alkali chloride. An apparent K_1K_2 was plotted as a function of ionic strength and extrapolated to infinite dilution to eliminate activity coefficient corrections and to obtain the true value of K_1K_2. The value of this method lies in the fact that the molality term is insensitive to relatively large uncertainties in the hydrolysis correction. In applying this procedure to a resolution of the dissociation constants of tartaric acid, Bates and Canham [15] evaluated the second constant with the aid of approximate values for the first. The product K_1K_2 was then evaluated and a new, more precise, value of K_1 was computed.

2. Method

It seemed worthwhile to explore the possibility of modifying the Speakman method to permit the simultaneous determination of the dissociation constants of a dibasic acid with a precision comparable with that obtainable by the "conventional" method for a single isolated dissociation step. To this end, the equations were formulated in terms of $f_H f_{Cl} m_H$ (that is, $\mathbf{a}_H f_{Cl}$) instead of $\mathbf{a}_H$, since the former can be derived unambiguously from measurements of the emf of cell (1) by means of eq (2). This quantity will be termed P:

$$P \equiv \mathbf{a}_H f_{Cl} = f_H f_{Cl} m_H \qquad (5)$$

2.1. Overlapping Dissociation

The malate buffer solutions were all prepared from potassium hydrogen malate with the addition of perchloric acid or potassium hydroxide as desired. It was convenient to define two new quantities as follows:

α=the amount of potassium hydrogen malate used, in moles per kg of water.

β=the amount of strong acid used, in moles per kg of water. If strong base is added instead of strong acid, the sign of β is negative.

The potassium chloride present in all solutions at a molality of 0.008 must, of course, enter into the computation of the ionic strength. It does not, however, participate in the dissociation equilibria of malic acid, and it is therefore omitted in the following derivation of the relationships among P, α, β, K_1, and K_2.

From the requirement of electroneutrality, we have the following condition:

$$[K^+]+[H^+]=[ClO_4^-]+[OH^-]+[HMal^-]+2[Mal^=], \quad (6)$$

where $HMal^-$ and $Mal^=$ are written for the hydrogen malate and malate ions, respectively, and where the quantity in brackets represents the molality of the particular species of ion. It is convenient to define a quantity B as follows:

$$B\equiv\beta-[H^+]+[OH^-]. \quad (7)$$

It will be noted that for all the malate buffer solutions

$$[K^+]-[ClO_4^-]=\alpha-\beta. \quad (8)$$

From eq (6), (7), and (8), therefore,

$$\alpha-B=[HMal^-]+2[Mal^=]. \quad (9)$$

It can also be shown that

$$\alpha+B=2[H_2Mal]+[HMal^-]. \quad (10)$$

These relationships can now be combined with the equations for the two thermodynamic constants, K_1 and K_2, of malic acid. In this way, an equation analogous to that of Speakman [17] is derived.

2.2. Resolution of K_1 and K_2

Unfortunately, Speakman's equation cannot be applied in an exact way to the determination of overlapping dissociation constants, inasmuch as there is no known experimental means of measuring hydrogen ion activities. The closely related function P, however, possesses the thermodynamic validity that $\mathbf{a}_H$ lacks. With the further substitution of $\mathbf{a}_H=P/f_{Cl^-}$ one obtains

$$P^2\frac{\alpha-B}{\alpha+B}\cdot\frac{f_{A^=}}{f_{H_2A}f_{Cl^-}^2}=P\frac{B}{\alpha+B}\cdot\frac{f_{A^=}}{f_{HA^-}f_{Cl^-}}K_1+K_1K_2, \quad (11)$$

which may be written

$$Y=X\sigma K_1+(K_1K_2)/\rho \quad (12)$$

where

$$X\equiv\frac{PB}{\alpha+B}, \quad (13)$$

and

$$Y\equiv\frac{P^2(\alpha-B)}{\alpha+B}, \quad (14)$$

and in which the activity coefficient terms are

$$\sigma\equiv\frac{f_{H_2A}f_{Cl^-}}{f_{HA^-}} \quad (15)$$

and

$$\rho\equiv\frac{f_{A^=}}{f_{H_2A}f_{Cl^-}^2}. \quad (16)$$

Apart from the correction for the concentration of free hydrogen or hydroxyl ions in the buffer solutions in the computation of B by eq (7) (see below), the quantities X and Y can be derived without difficulty from the stoichiometric molalities and the measured emf of cells of type (1). This correction is usually small, for the experimental conditions can often be so arranged that α and β are large compared with m_H and m_{OH}.

It can be seen that eq (12) will be linear in X and Y if certain conditions can be met, namely: if the different values of the independent variables do not appreciably effect the constancy of σ and $1/\rho$. Studies of salt effects indicate that the activity coefficient terms are often largely dependent on the ionic strength (μ) and not on the nature of the added salt [19, 20]. Therefore, it should be justifiable to consider σ and ρ constant, within the error of the determination, when comparing values of X and Y derived from the measurement of solutions containing different ratios of acid salt to strong acid (or strong base) at constant ionic strength. This treatment of salt effects appears to be adequate in malate buffers, because a straight line was obtained for each value of the ionic strength when Y was plotted as a function of X. The slope of each line is σK_1 and the intercept is (K_1K_2/ρ).

Fortunately, activity-coefficient terms of the same type as σ are often close to unity in the regions of low and intermediate ionic strength ($\mu<0.1$).[4] At $\mu=0.06$, σ was found to be 0.96. Furthermore, log σ shows the expected linear variation with ionic strength, and consequently the curves obtained by plotting log (σK_1) against ionic strength were easily extrapolated to zero ionic strength. Since σ approaches unity at infinite dilution, the intercept for $\mu=0$ is log K_1.

[4] In buffer solutions composed of equimolal amounts of acetic acid, sodium acetate, and sodium chloride, log $(f_{HAc}f_{Cl}/f_{Ac})$ is given by $-0.06\,\mu$; in acetate buffers containing potassium iodide, log $(f_{HAc}f_I/f_{Ac})$ is $-0.14\,\mu$ [21].

Similarly, log K_2 is obtained by extrapolating log (K_2/ρ) to zero ionic strength. An activity-coefficient term of the charge type of ρ, however, cannot be expected to be very near unity at moderate ionic strengths (ρ was found to be about 0.6 at the highest ionic strengths included in this study), nor can log ρ be expected to vary linearly with ionic strength. In order to correct the curvature of the lines and to facilitate the extrapolation, estimated values of ρ (designated ρ^*) were computed from the Debye-Hückel formula

$$\log \rho^* = \frac{-2A\sqrt{\mu}}{1+6.25B\sqrt{\mu}}, \tag{17}$$

where A and B are constants of the Debye-Hückel theory [22]. The quantity log $\rho^*(K_2/\rho)$, instead of log K_2/ρ, was then plotted as a function of μ. Several values for the coefficient of the $B\sqrt{\mu}$ term in the denominator of eq (17) were tried, and 6.25 was found to furnish the best linear plot of log $\rho^*(K_2/\rho)$ as a function of μ. The lines obtained were readily extended to zero ionic strength, where $\rho^*(K_2/\rho)$ becomes equal to K_2.

2.3. Computation of B

In order to utilize eq (11) or (12) to resolve K_1 and K_2 as described in the preceding section, two other quantities, B and μ, must be known. The former can be obtained readily from β, the stoichiometric molality of strong acid or base, by eq (7), together with $[H^+]$ and $[OH^-]$. Inasmuch as the pH range of malate buffers extends from about 2.5 to 6.0, the concentration of hydroxyl ion is always less than 1 percent of m_H and can be neglected. Hence,

$$B \approx \beta - [H^+]. \tag{7a}$$

2.4. Hydrogen Ion Concentration

Values of the molality of hydrogen ion, $[H^+]=m_H$, were derived directly from the emf by eq (2); $f_H f_{Cl}$ is (by definition) equal to f_{HCl}^2, the square of the mean ionic molal activity coefficient of hydrocloric acid in the malate-chloride buffer solution. Values of f_{HCl} in pure aqueous solutions of hydrochloric acid of the same ionic strength as the malate-chloride buffer solutions were used in the computation of $[H^+]$. They were taken from Harned and Ehlers [4, 23].

2.5. The Ionic Strength

With the aid of eq (9) it can be shown that the ionic strength of the solutions containing acid salt (KHMal) and potassium chloride ($m=0.008$), or these components with added strong acid, is given by

$$\mu = 0.008 + \alpha + m_H + m_{Mal^=}, \tag{18}$$

inasmuch as the hydroxyl ion concentration is negligibly small.

When the solutions contain potassium chloride (0.008 m), potassium hydrogen malate, and potassium hydroxide (stoichiometric molality of $-\beta$), the ionic strength is

$$\mu = 0.008 + \alpha - 2\beta + 2m_H + m_{H_2Mal} \tag{19}$$

In order to calculate the ionic strength by these two equations, it was necessary to evaluate the molalities of malic acid and bivalent malate ion as well as that of hydrogen ion. These quantities can only be obtained through successive approximations, as values of the ionic strength and also of the approximate dissociation constants must be used in their computation. However, all were small relative to α, and usually to β also, so that the approximations converged rapidly.

The molality of malate ion, needed to calculate the ionic strength by eq (18), can be expressed by

$$m_{Mal^=} = \frac{K_1K_2}{\rho I^2}(\beta - m_H + m_{Mal^=}) \tag{20}$$

with the aid of eq (5), (7a), and (16). In the solutions of acid salt, to which no strong acid or strong base has been added, β is zero and consequently

$$m_{Mal^=} = \frac{-K_1K_2m_H}{\rho I^2 - K_1K_2}. \tag{21}$$

In the solutions to which perchloric acid had been added, β was large compared with m_H and $m_{Mal^=}$; hence,

$$m_{Mal^=} \approx \frac{K_1K_2\beta}{\rho I^2}. \tag{21a}$$

When the solutions contained added strong alkali, it was necessary to estimate the molality of free malic acid in order to compute the ionic strength by eq (19). From eq (5), (7a), (10), and (15),

$$m_{H_2Mal} = \frac{[P/(\sigma K_1)](\alpha + \beta - m_H)}{1+[2P/(\sigma K_1)]}. \tag{22}$$

When strong alkali had been added to the solution of acid salt, $2P/\sigma K_1$ was much less than unity. Furthermore, σ is nearly unity at low and intermediate ionic strengths; hence,

$$m_{H_2A} \approx \frac{P}{K_1}(\alpha + \beta - m_H). \tag{22a}$$

The accurate evaluation of m_{H_2Mal} and $m_{Mal^=}$ as described above is quite evidently a laborious procedure. However, neither of these quantities makes a large contribution to the ionic strength obtained by eq (18) and (19), and therefore accurate values are unnecessary. Consequently, the following procedure was followed: A preliminary value of the ionic strength was derived with the omission of the last two terms of eq (18) and (19), and a first approximation to m_H was made, which led to a more accurate

value of μ by eq (18) and (19), the last term of each of these equations being omitted.

The first approximation to $m_{\mathrm{Mal}^=}$ and $m_{\mathrm{H_2Mal}}$ was then made by eq (21), (21a), or (22a), the choice being dependent on the composition of the buffer solution. For this purpose, the values of K_1 and K_2 could be obtained with sufficient accuracy from the literature, from titration curves, or from a preliminary plot of Y as a function of X. The ionic strength was now recalculated, a new value of m_{H} obtained, and the process repeated until a consistent set of values resulted.

3. Experimental Procedures

Potassium hydrogen malate was prepared from reagent-grade *d,l*-malic acid and potassium bicarbonate. A solution of the salt was decolorized at 60° C with activated charcoal. The filtrate was cooled in a water-ice bath and the crude salt precipitated by the addition of ethanol. This precipitate was recrystallized five times from ethanol-water mixtures. The salt collected after the fifth crystallization was dried overnight at 130° C in air.

The potassium hydrogen malate was assayed by titration with the standard solution of potassium hydroxide described below. After the first recrystallization, the dried salt was found to assay 99.69 percent potassium hydrogen malate. After the third recrystallization, the assay was 99.99 percent.

Potassium chloride was prepared according to the procedure outlined by Pinching and Bates [24].

The standard carbonate-free solution of potassium hydroxide (0.1 molal) was standardized against potassium hydrogen phthalate (NBS Standard Sample 84b) in a carbon dioxide-free atmosphere. Weight burettes were used. This alkali solution was used both for titrations and for the preparation of the cell solutions.

Reagent-grade perchloric acid, 70 percent by weight, was diluted with conductivity water to make a solution of molality about 0.1. The acid solution was standardized against the potassium hydroxide solution. It was tested for the presence of chloride with silver nitrate solution according to the procedure described by Rosin [25] and was found to contain less than 0.001 percent.

Eight stock solutions of malate buffers were prepared. Additional cell solutions were prepared by diluting these with an 0.008-*m* solution of potassium chloride. The compositions of the solutions appear in the second and third columns of table 1.

TABLE 1. *Values of log* $(-f_{\mathrm{H}}fclm_{\mathrm{H}})$ *derived from emf measurements of cell (1)*

Series	α	β	$-\log (f_{\mathrm{H}}fclm_{\mathrm{H}})$ at temperature of—										
			0° C	5° C	10° C	15° C	20° C	25° C	30° C	35° C	40° C	45° C	50° C
	moles/kg H_2O	(±)*moles kg* H_2O											
	0.06240	0.04365	3.1749	3.1556	3.1392	3.1265	3.1150	3.1061	3.0987	3.0942	3.0923	3.0940	3.0951
	.04153	.02805	3.1881	3.1704	3.1554	3.1431	3.1315	3.1226	3.1153	3.1117	3.1096	3.1111	3.1127
1	.02105	.014724	3.2229	3.2057	3.1918	3.1793	3.1685	3.1600	3.1536	3.1496	3.1477	3.1499	3.1499
	.013431	.009395	3.2608	3.2423	3.2289	3.2212	3.2148	3.2035	3.1970	3.1916	3.1859	3.1870	3.1886
	.005893	.004122	3.3355	3.3325	3.3121	3.3016	3.2944	3.2878	3.2811	3.2774	3.2761	3.2784	3.2806
	.05398	.03402	3.2720	3.2515	3.2353	3.2225	3.2115	3.2044	3.1968	3.1933	3.1913	3.1928	3.1958
	.03572	.02251	3.2800	3.2597	3.2440	3.2314	3.2208	3.2126	3.2059	3.2024	3.2001	3.2020	3.2039
2	.02025	.012764	3.3086	3.2878	3.2739	3.2617	3.2513	3.2436	3.2370	3.2337	3.2320	3.2332	3.2353
	.011394	.007182	3.3424	3.3245	3.3094	3.2985	3.2892	3.2822	3.2771	3.2743	3.2738	3.2746	3.2757
	.05403	.019861	.....	3.6709	3.6545	3.6418	3.6313	3.6231	3.6174	3.6143	3.6118	3.6150	3.6171
	.03560	.013087	.....	3.6808	3.6642	3.6519	3.6412	3.6327	3.6262	3.6236	3.6208	3.6226	3.6241
3	.018463	.006787	.....	3.6931	3.6774	3.6655	3.6549	3.6467	3.6403	3.6383	3.6359	3.6392	3.6428
	.012235	.004498	.....	3.7059	3.6916	3.6802	3.6697	3.6611	3.6552	3.6530	3.6507	3.6537	3.6563
	.005282	.0019417	.....	3.7445	3.7304	3.7204	3.7109	3.7070	3.6991	3.6973	3.6955	3.6980	3.7024
	.05444	0	4.2450	4.2284	4.2143	4.2054	4.1978	4.1939	4.1882	4.1878	4.1909	4.1977	4.2056
	.05314	0	4.2454	4.2288	4.2141	4.2038	4.1964	4.1921	4.1895	4.1912	4.1945	4.2012	4.2090
	.03563	0	4.2576	4.2411	4.2278	4.2184	4.2107	4.2040	4.2013	4.2009	4.2030	4.2088	4.2166
	.03469	0	4.2543	4.2384	4.2241	4.2141	4.2065	4.2021	4.1995	4.2005	4.2041	4.2118	4.2198
	.02244	0	4.2651	4.2491	4.2363	4.2278	4.2209	4.2170	4.2141	4.2148	4.2178	4.2249	4.2332
4	.02069	0	4.2653	4.2482	4.2346	4.2249	4.2177	4.2146	4.2131	.....	.....	.....	.....
	.012406	0	4.2792	4.2630	4.2500	4.2415	4.2353	4.2319	4.2293	4.2302	4.2334	4.2406	4.2485
	.011267	0	4.2805	4.2641	4.2499	4.2403	4.2330	4.2280	4.2246	4.2249	4.2286	4.2355	4.2436
	.005193	0	4.2995	4.2830	4.2712	4.2627	4.2562	4.2535	4.2505	4.2519	4.2564	4.2648	4.2759
	.004721	0	4.2984	4.2825	4.2704	4.2625	4.2566	4.2530	4.2505	4.2511	4.2537	4.2595	4.2700
	.03027	−0.012114	4.8546	4.8442	4.8331	4.8279	4.8231	4.8220	4.8221	4.8275	4.8346	4.8459	4.8583
	.02003	−.008016	4.8740	4.8616	4.8523	4.8479	4.8430	4.8411	4.8429	4.8482	4.8555	4.8670	4.8800
5	.010129	−.004054	4.8939	4.8813	4.8719	4.8674	4.8632	4.8577	4.8624	4.8682	4.8761	4.8877	4.8996
	.006440	−.002577	4.9054	4.8942	4.8858	4.8807	4.8759	4.8758	4.8778	4.8836	4.8917	4.9033	4.9146
	.002819	−.0011282	4.9385	4.9111	4.9030	4.8984	4.8936	4.8945	4.8975	4.9032	4.9107	4.9224	4.9364
	.03034	−.012624	4.8880	4.8741	4.8632	4.8566	4.8524	4.8522	4.8529	4.8578	4.8653	4.8767	4.8875
	.019568	−.008142	4.8921	4.8781	4.8678	4.8627	4.8721	4.8608	4.8602	4.8640	4.8721	4.8837	4.8964
6	.011054	−.004600	4.9238	4.9107	4.9004	4.8946	4.8921	4.8912	4.8928	4.8991	4.9073	4.9195	4.9316
	.006819	−.002837	4.9284	4.9151	4.9052	4.9000	4.8973	4.8966	4.8988	4.9055	4.9139	4.9296	4.9385
	.002983	−.0012412	4.9613	4.9488	4.9390	4.9332	4.9299	4.9294	4.9314	4.9382	4.9463	4.9592	4.9715
	.02319	−.015322	5.2845	5.2695	5.2591	5.2529	5.2493	5.2489	5.2509	5.2570	5.2652	5.2775	5.2909
	.017223	−.011379	5.3055	5.2902	5.2781	5.2747	5.2713	5.2716	5.2741	5.2808	5.2897	5.3019	5.3150
7	.009695	−.006405	5.3200	5.3041	5.2936	5.2887	5.2862	5.2868	5.2894	5.2958	5.3043	5.3170	5.3297
	.007129	−.004710	5.3322	5.3183	5.3086	5.3029	5.2983	5.2983	5.3001	5.3049	5.3139	5.3264	5.3404
	.004592	−.003034	5.3435	5.3312	5.3225	5.3168	5.3141	5.3141	5.3174	5.3252	5.3343	5.3472	5.3608

The apparatus and the experimental procedures employed in this work were essentially as described by Bates and Acree [26]. The temperature of the bath containing the cells was maintained within $\pm 0.02°$ C of the nominal temperatures. The temperature sequence used, with a few exceptions, was 25°, 15°, 5°, 0°, 10°, 20°, 30°, 40°, 50°, 45°, 35°, and 25° C. Individual emf readings were discarded if the cell potential varied by more than 0.2 mv from the smooth curve obtained by plotting emf against temperature. All measured values for a given solution were discarded if the final value of 25° C differed from the initial value by more than 0.3 mv.

The cells usually attained their equilibrium values in about 30 min after each change in temperature. Equilibrium was judged to have been reached when readings of the same set of electrodes taken 10 min apart differed by 0.03 mv or less.

4. Results and Calculations

The values of $-\log (f_H f_{Cl} m_H)$ for each solution from 0° to 50° C are assembled in table 1. The solutions were composed of potassium hydrogen malate (molality α) and potassium chloride (molality 0.008), and some of them also contained perchloric acid or potassium hydroxide (molality $\pm\beta$). A positive value of β signifies the presence of perchloric acid, whereas a negative value indicates that potassium hydroxide had been added. Each figure for $-\log (f_H f_{Cl} m_H)$ represents the mean value derived from the two pairs of electrodes in the same cell.

4.1. Calculation of K_1

The quantities X and Y, computed by means of eq (13) and (14), were plotted as a function of ionic strength. Different curves were obtained for each series of solutions and for the same series at different temperatures. Two representative plots are shown in figures 1 and 2. The values of X and Y corresponding to ionic strengths of 0.06, 0.05, 0.04, 0.03, 0.025, 0.02, and 0.014 were obtained by interpolation on each curve.

A second series of graphs was prepared, in which Y was plotted as a function of X at each of the seven values of the ionic strength and at each of the 11 temperatures. These plots consisted of straight lines, as shown in figure 3. The position of each line was determined by the method of least squares. The logarithm of the *slope* (σK_1) of these lines was next plotted as a function of ionic strength at each temperature (compare fig. 4). The least-squares straight line drawn through the points was extended to $\mu = 0$, where $\log \sigma K_1 = \log K_1$. The mean deviation of the individual values of $\log \sigma K_1$ from the line was ± 0.0010 unit. The values of $\log K_1$ obtained in this way are summarized in table 2.

4.2. Calculation of K_2

The second dissociation constant was derived from the *intercepts* ($K_1 K_2/\rho$) of the plots of Y with respect to X. If the experimental errors for all of the meas-

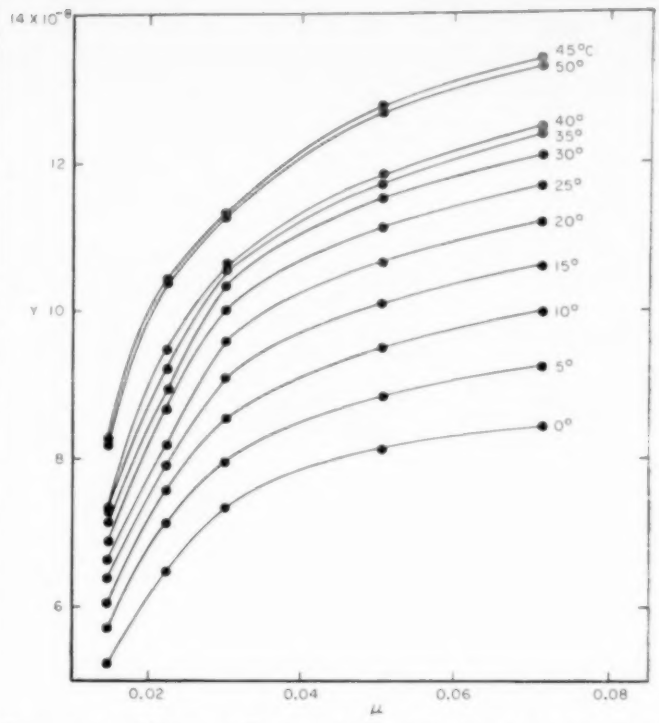

FIGURE 1. *Values of X from 0° to 50° C plotted as a function of ionic strength.*

Series 1.

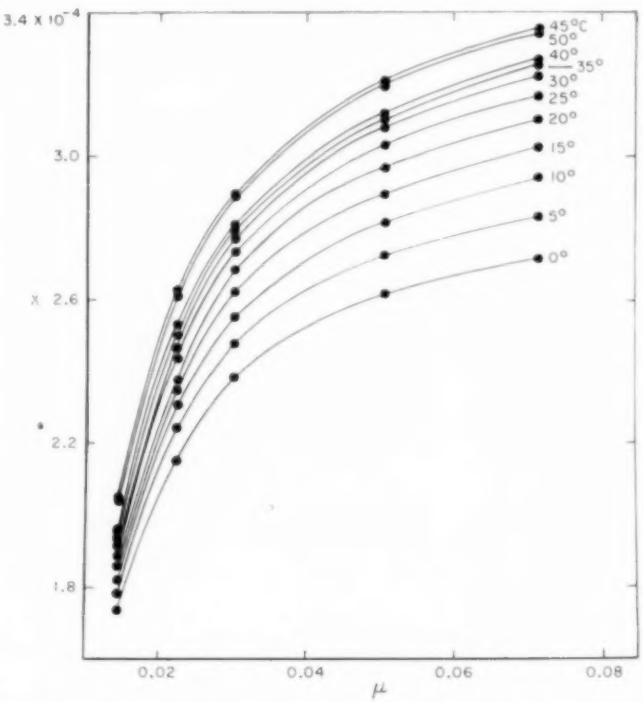

FIGURE 2. *Values of Y from 0° to 50° C plotted as a function of ionic strength.*

Series 1.

ured points were about equal in magnitude, it is to be expected that the best values of the intercept would be obtained by the shortest extrapolations. For this reason, only the data derived from the four series (4 through 7) composed of the least acidic solutions ($\beta \leq 0$) with the smallest values of X and Y were used to derive K_2. The value of K_1K_2/ρ corresponding to each of these experimental points was

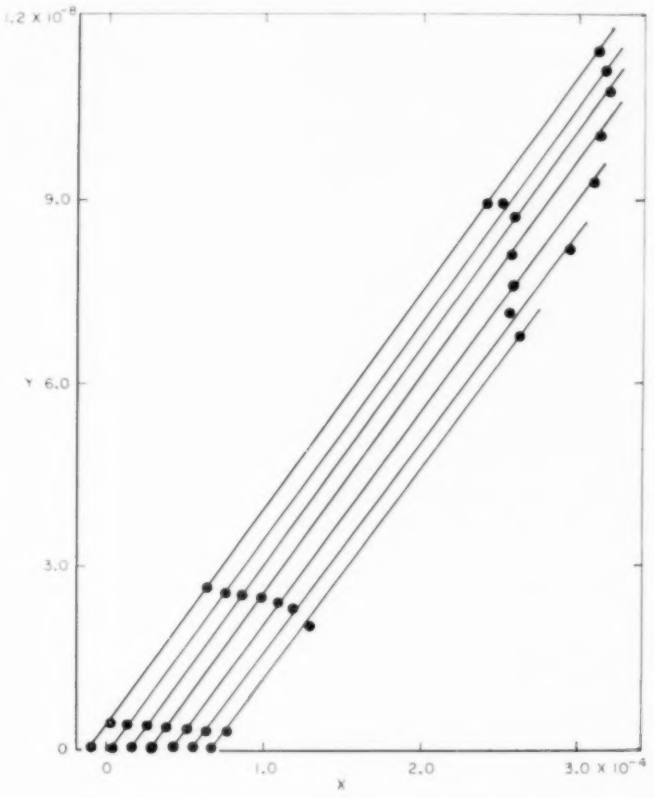

FIGURE 3. *Plots of Y versus X at 25° C.*

From left to right, the lines correspond to ionic strengths of 0.06, 0.05, 0.04, 0.03, 0.025, 0.020, and 0.014. The axis of ordinates has been transposed to the right by 0.125 unit for each successive member.

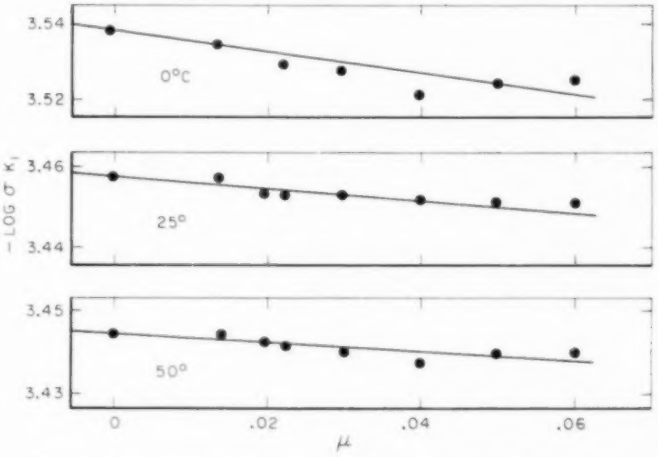

FIGURE 4. *Plots of $-\log \sigma K_1$ at 0°, 25°, and 50° C as a function of ionic strength.*

TABLE 2. *Summary of log K_1 and K_1 from 0° to 50° C*

Temperature	$-\log K_1$	$K_1 \times 10^4$
° C		
0	3.537$_7$	2.90
5	3.520$_2$	3.02
10	3.494$_3$	3.20
15	3.482$_5$	3.29
20	3.472$_3$	3.37
25	3.458$_6$	3.48
30	3.452$_0$	3.53
35	3.446$_9$	3.57
40	3.444$_0$	3.60
45	3.446$_7$	3.58
50	3.445$_2$	3.59

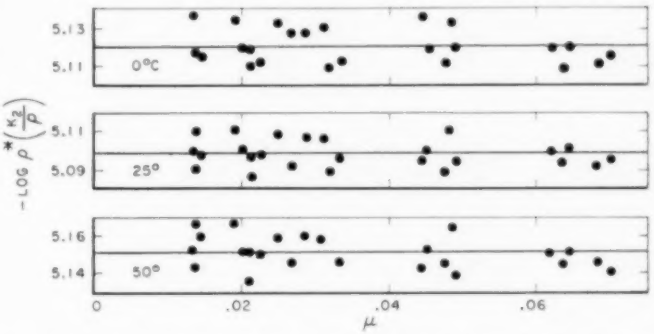

FIGURE 5. *Plots of $-\log \rho^*(K_2/\rho)$ at 0°, 25°, and 50° C as a function of ionic strength.*

computed from the individual values of X and Y, together with the slope of the appropriate X, Y plot determined by the method of least squares.

The values of $\log \rho^*(K_2/\rho)$ were independent of ionic strength, within experimental error, as can be seen in figure 5. It appears, therefore, that ρ^* calculated by eq (17) is a very good representation of ρ at these ionic strengths, and it follows that $\rho^*(K_2/\rho)$ is equal to K_2. The mean values of $\log K_2$ at each temperature are summarized in table 3. An arbitrary weight of 2 was assigned to those values computed from the 10 solutions (series 4) which contained neither strong acid nor strong base. For these solutions, β was 0. The values of X were consequently small, and errors in establishing the slope of the X, Y line had only a slight influence on the intercepts obtained.

TABLE 3. *Summary of log K_2 and K_2 from 0° to 50° C*

Temperature	Number of solutions	$-\log K_2$	Standard deviation of mean	$K_2 \times 10^5$
° C				
0	25	5.119$_4$	0.0014	7.60
5	25	5.108$_5$	.0014	7.79
10	25	5.098$_8$	.0013	7.97
15	25	5.096$_0$	.0013	8.02
20	25	5.096$_2$	.0012	8.01
25	25	5.097$_4$	.0012	7.99
30	25	5.099$_5$	.0012	7.95
35	24	5.104$_3$	.0015	7.86
40	24	5.117$_9$	.0014	7.62
45	24	5.133$_9$	.0014	7.36
50	24	5.149$_4$	.0015	7.09

4.3. Dissociation Constants and Temperature

The values of log K_1 and log K_2 can be expressed by the equation suggested by Harned and Robinson [27], namely

$$-\log K=\frac{A}{T}+B+CT \tag{23}$$

The parameters A, B, and C were determined by the method of least squares, and the following results were obtained:

$$-\log K_1=\frac{1358.85}{T}-5.1382+0.013550\ T \tag{24}$$

and

$$-\log K_2=\frac{1658.53}{T}-6.2364+0.019353\ T, \tag{25}$$

where T is the temperature on the Kelvin scale. The average differences between the "observed" values of log K_1 and log K_2 at the 11 temperatures and the corresponding values calculated by eq (24) and (25) were 0.0013 unit and 0.0011 unit, respectively.

4.4. Comparison With Earlier Work

A considerable number of determinations of the dissociation constants of malic acid has been made in the last half century. The values obtained by these earlier workers have been assembled in table 4. The columns headed K_1' and K_2' list values of the "concentration constants", uncorrected for activity coefficients. The columns headed K_1 and K_2 give values for the thermodynamic constants. Unless the author made a definite statement that activity coefficients had been used to correct the equilibrium equations, it was assumed that the dissociation constants had been calculated on a concentration basis. The values of the "concentration" dissociation constants K_1' and K_2' listed in table 4 are uniformly higher than the thermodynamic dissociation constants. This is to be expected, since the activity-coefficient correction would decrease the value of the dissociation constant in dilute solutions.

It is clear from table 4 that agreement between the results of various workers is much better for the first constant than for the second constant. All of the earlier values of K_2 are somewhat lower than those found in this investigation. Only the electrometric determination of K_2 by Larsson [28] agrees well with the value reported here. No statement can be made about the relative accuracy of these earlier determinations of K_2.

5. Thermodynamics of the Dissociation Processes

The thermodynamic quantities associated with the two dissociation steps were computed by the following equations:

$$\Delta G^\circ=2.3026\ R(A+BT+CT^2) \tag{26}$$
$$\Delta H^\circ=2.3026\ R(A-CT^2) \tag{27}$$
$$\Delta S^\circ=-2.3026\ R(B+2CT) \tag{28}$$
$$\Delta C_p^\circ=-2.3026\ R(2CT) \tag{29}$$

where R is the gas constant, 8.31439 j deg^{-1}mole^{-1}. The thermodynamic constants are summarized in table 5.

TABLE 4. *Summary of reported values of the first and second dissociation constants of malic acid*

Author	Year	Method	Temperature	$K_1'\times10^4$	$K_1\times10^4$	$K_2'\times10^6$	$K_2\times10^6$	Reference
			°C					
Ostwald	1889	Conductance	25	3.95	.....	.....	.....	[29]
Ostwald	1889	....do	25	3.99	.....	.....	.....	[29]
Berthelot	1891	....do	17	3.83	.....	.....	.....	[30]
Walden	1896	....do	25	4.0	.....	.....	.....	[31]
Smith	1898	Inversion of sucrose	100	[a] 3.99	.....	8.3	.....	[32]
Wegscheider	1902	Conductance	17	[a] 4.0	.....	7.5	.....	[33]
Dhar and Datta	1913	Solubility	.....	.....	.....	9.0	.....	[34]
Larsson	1922	emf	18	[a] 4.0	.....	.....	7.8	[35]
Auerbach and Smolczyk	1924	....do	20	3.86	.....	13.9	.....	[6]
Bjerrum	1924	....do	15	4.0	.....	.....	.....	[36]
Coops	1924	Conductance	25	3.76	.....	.....	.....	[37]
Larsson	1924	....do	15	.....	3.32	.....	.....	[38]
Larsson	1924	....do	18	[a] 4.0	.....	.....	6.9	[28]
Roth and Wilms	.....	....do	25	3.93	.....	.....	.....	[39]
Mizutani	1925	emf	18	4.7	.....	13.5	.....	[40]
Larsson	1926	Solubility	25	[a] 4.0	.....	.....	7.3	[41]
Duboux and Frommelt	1927	Rate of decomposition of diazoacetic ester.	25	[a] 3.95	.....	.....	7.4	[42]
This investigation	.....	emf without liquid junction	15	.....	3.29	.....	8.02	.....
			20	.....	3.37	.....	8.01	.....
			25	.....	3.48	.....	7.99	.....

[a] The value of K_1 was obtained from the data of Ostwald [29] and used to calculate K_2.

TABLE 5. *Thermodynamic quantities for the dissociation of malic acid and hydrogen malate ion from 0° to 50° C*

Temperature	$\Delta G°$	$\Delta H°$	$\Delta S°$	$\Delta C_p°$
Process: $H_2Mal \rightleftharpoons H^+ + HMal^-$				
°C	j mole^{-1}	j mole^{-1}	j deg^{-1} mole^{-1}	j deg^{-1} mole^{-1}
0	18,510	6,662	−43.4	−142
5	18,730	5,946	−46.0	−144
10	18,970	5,219	−48.6	−147
15	19,220	4,477	−51.2	−150
20	19,480	3,723	−53.7	−152
25	19,750	2,955	−56.3	−155
30	20,040	2,176	−58.9	−157
35	20,340	1,381	−61.5	−160
40	20,680	576	−64.1	−163
45	20,980	−243	−66.7	−165
50	21,330	−1,076	−69.3	−168
Process: $HMal^- \rightleftharpoons H^+ + Mal^=$				
0	26,780	4,112	−82.9	−203
5	27,210	3,089	−86.6	−206
10	27,650	2,049	−90.3	−210
15	28,120	990	−94.0	−214
20	28,590	−276	−97.7	−217
25	29,090	−1,181	−101.4	−221
30	29,610	−2,296	−105.1	−225
35	30,120	−3,428	−108.8	−228
40	30,680	−4,579	−112.6	−232
45	31,250	−5,751	−116.2	−236
50	31,840	−6,940	−120.0	−240

6. Discussion

It is of interest to compare the dissociation constants and associated thermodynamic quantities for the three structurally related acids, succinic, malic and tartaric. The constants A, B, and C of eq (23) for the dissociation constants of these three acids are as follows:

		A	B	C
K_1	Succinic acid	1206.25	−3.3266	0.011697
	Malic acid	1358.85	−5.1382	.013550
	Tartaric acid	1525.59	−6.6558	.015336
K_2	Succinic acid	1679.13	−5.7043	.019153
	Malic acid	1658.53	−6.2364	.019353
	Tartaric acid	1765.35	−7.3015	.019276

A comparison of the thermodynamic data derived from these constants is presented in table 6.

It is noted first of all that progressive substitution of hydroxy groups on the two middle carbons enhances the strength of both acidic groups. This effect is the expected one. Thus, the value of —log K for glycolic acid [43] is 0.9 unit lower than that for acetic acid [2, 44], and that for lactic acid [45] is lower by 1.0 unit than that for propionic acid [46]. The decreases are somewhat smaller for both steps in the dissociation of the dibasic acids.

The interpretation of the changes of entropy and heat capacity associated with the dissociation of weak dibasic acids is not simple. Statistical, electrostatic, and structural factors have been discussed by Everett and his coworkers [47, 48]. It is likely that orientation of solvent molecules in the electrostatic field adjacent to the ions plays an important role in determining the sign and to some extent the magnitude of the changes of entropy and heat capacity when an acid dissociates.[5] Structural features leading to "screening" or solvent exclusion have an opposite effect. When the dissociation produces an increase of charge, as it does with uncharged acids and with acid anions, the increased solvent orientation and attendant immobilization of solvent molecules should bring about a decrease in both heat capacity and entropy. Indeed, $\Delta S°$ and $\Delta C_p°$ for acids of these types are almost invariably negative.

Although solvent orientation is recognized as a factor of primary importance, other factors often outweigh its effect, as shown by the contrary variation of $\Delta S°$ and $\Delta C_p°$ with chain length in a series of acids of the same charge type [47], and by the fact that the values of $\Delta S°$ for the dissociation of some cationic acids are negative while $\Delta C_p°$ is positive [51, 52]. At the present time, even qualitative predictions are often of little value.

It is nevertheless worthwhile to compare the observed values of these thermodynamic quantities for acids of like structure, to note the similarities, and to attempt to explain the differences. The constancy of $\Delta C_p°$ for the second dissociation steps is perhaps the most striking feature of the comparison given in table 6. The regular increase of $\Delta S°$ from succinic acid to tartaric acid suggests that progressive substitution of the two carbon atoms lying between the carboxyl groups is accompanied by an increased exclusion of solvent molecules. The concomitant decrease of $\Delta C_p°$ for the first dissociation step is also regular, but the reason for a change in this direction is not readily apparent.

[5] See, for example, references [49] and [50].

TABLE 6. *Comparison of the thermodynamic constants for the two dissociation steps of succinic, malic, and tartaric acids at 25° C*

Acid	First step				Second step			
	$-\log K_1$	$\Delta H°$	$\Delta S°$	$\Delta C_p°$	$-\log K_2$	$\Delta H°$	$\Delta S°$	$\Delta C_p°$
		j mole^{-1}	j deg^{-1} mole^{-1}	j deg^{-1} mole^{-1}		j mole^{-1}	j deg^{-1} mole^{-1}	j deg^{-1} mole^{-1}
[a] Succinic $COOH\text{-}CH_2\text{-}CH_2\text{-}COOH$	4.207	3,186	−70	−134	5.636	−450	−109	−219
Malic $COOH\text{-}CHOH\text{-}CH_2\text{-}COOH$	3.459	2,955	−56	−155	5.097	−1181	−101	−221
[b] Tartaric $COOH\text{-}CHOH\text{-}CHOH\text{-}COOH$	3.036	3,100	−48	−170	4.366	990	−80	−220

[a] Pinching and Bates [14, 53].
[b] Bates and Canham [15].

7. References

[1] E. J. Roberts, J. Am. Chem. Soc. **52,** 5079 (1930).
[2] H. S. Harned and R. W. Ehlers, J. Am. Chem. Soc. **54,** 1350 (1932).
[3] R. G. Bates, J. Research NBS **47,** 127 (1951) RP2236.
[4] H. S. Harned and R. W. Ehlers, J. Am. Chem. Soc. **55,** 2179 (1933).
[5] R. G. Bates and G. D. Pinching, J. Research NBS **42,** 419 (1949) RP1982.
[6] F. Auerbach and E. Smolczyk, Z. physik. Chem. (Leipzig) **110,** 65 (1924).
[7] H. S. Simms, J. Am. Chem. Soc. **48,** 1239 (1926).
[8] C. Morton, Trans. Faraday Soc. **24,** 14 (1928).
[9] S. Glasstone, Introduction to electrochemistry, pp. 325 ff. (D. Van Nostrand, New York, N.Y., 1942).
[10] H. T. S. Britton, J. Chem. Soc. **127,** 1896 (1925).
[11] N. Bjerrum and A. Unmack, Kgl. Danske Videnskab. Selskab., Math-fys Medd. **9,** No. 1 (1929).
[12] W. J. Hamer and S. F. Acree, J. Research NBS **35,** 381 (1945) RP1678.
[13] W. J. Hamer, G. D. Pinching, and S. F. Acree, J. Research NBS **35,** 539 (1945) RP1687.
[14] G. D. Pinching and R. G. Bates, J Research NBS **45,** 322 (1950) RP2142.
[15] R. G. Bates and R. G. Canham, J. Research NBS **47,** 343 (1951) RP2260.
[16] R. G. Bates and G. D. Pinching, J. Am. Chem. Soc. **71,** 1274 (1949).
[17] J. C. Speakman, J. Chem. Soc. **1940,** 855.
[18] R. G. Bates, J. Am. Chem. Soc. **70,** 1579 (1948).
[19] R. G. Bates, P. T. Diamond, M. Eden, and S. F. Acree, J. Research NBS **37,** 251 (1946) RP1746.
[20] R. G. Bates, Electrometric *p*H determinations, ch. 5 (John Wiley & Sons, Inc., New York, N.Y., 1954).
[21] R. G. Bates, Chem. Revs. **42,** 1 (1948).
[22] G. G. Manov, R. G. Bates, W. J. Hamer, and S. F. Acree, J. Am. Chem. Soc. **65,** 1765 (1943).
[23] H. S. Harned and B. B. Owen, The physical chemistry of electrolytic solutions, 3d ed. (Reinhold Publishing Corp., New York, N.Y., 1958).
[24] G. D. Pinching and R. G. Bates, J. Research NBS **37,** 311 (1946) RP1749.
[25] J. Rosin, Reagent chemicals and standards, 2d ed. (D. Van Nostrand, New York, N.Y., 1946).
[26] R. G. Bates and S. F. Acree, J. Research NBS **30,** 129 (1943) RP1524.
[27] H. S. Harned and R. A. Robinson, Trans. Faraday Soc. **36,** 973 (1940).
[28] E. Larsson, quoted by J. N. Brønsted and K. Pedersen, Z. physik. Chem. (Leipzig) **108,** 185 (1924).
[29] W. Ostwald, Z. physik. Chem. (Leipzig) **3,** 369 (1889).
[30] D. Berthelot, Ann. chim. et phys. [6] **23,** 1 (1891).
[31] P. Walden, Ber. **29,** 1699 (1896).
[32] W. A. Smith, Z. physik. Chem. (Leipzig) **25,** 193 (1898).
[33] R. Wegscheider, Monatsh. **23,** 599 (1902).
[34] N. Dhar and A. K. Datta, Z. Elektrochem. **19,** 407 (1913).
[35] E. Larsson, Z. anorg. Chem. **125,** 281 (1922).
[36] N. Bjerrum, quoted by J. N. Brønsted and K. Pedersen, Z. physik. Chem. (Leipzig) **108,** 185 (1924).
[37] J. Coops, Dissertation Delft (1924), quoted in Landolt-Börnstein Physikalisch-Chemische Tabellen, 5th ed., 1er Ergbd, p. 650 (Berlin, 1927).
[38] E. Larsson, quoted by N. Bjerrum, Z. physik. Chem. (Leipzig) **106,** 219 (1924).
[39] W. A. Roth and Wilms, Unpublished data quoted in Landolt-Börnstein, Physikalisch-Chemische Tabellen, 5th ed., 1er Ergbd., p. 650 (Berlin, 1927).
[40] M. Mizutani, Z. physik. Chem. (Leipzig) **118,** 318 (1925).
[41] E. Larsson, Z. anorg. Chem. **155,** 247 (1926).
[42] M. Duboux and J. Frommelt, J. Chim. phys. **24,** 245 (1927).
[43] L. F. Nims, J. Am. Chem. Soc. **58,** 987 (1936).
[44] D. A. MacInnes and T. Shedlovsky, J. Am. Chem. Soc. **54,** 1429 (1932).
[45] L. F. Nims and P. K. Smith, J. Biol. Chem. **113,** 145 (1936).
[46] H. S. Harned and R. W. Ehlers, J. Am. Chem. Soc. **55,** 2379 (1933).
[47] D. H. Everett, D. A. Landsman, and B. R. W. Pinsent, Proc. Roy. Soc. (London) **[A] 215,** 403 (1952).
[48] D. H. Everett and B. R. W. Pinsent, Proc. Roy. Soc. (London) **[A] 215,** 416 (1952).
[49] D. D. Eley and M. G. Evans, Trans. Faraday Soc. **34,** 1093 (1938).
[50] D. H. Everett and C. A. Coulson, Trans. Faraday Soc. **36,** 633 (1940).
[51] D. H. Everett and W. F. K. Wynne-Jones, Proc. Roy. Soc. (London) **[A] 177,** 499 (1941).
[52] R. G. Bates and V. E. Bower, J. Research NBS **57,** 153 (1956) RP2705.
[53] G. D. Pinching and R. G. Bates, J. Research NBS **45,** 444 (1950) RP2156.

WASHINGTON, December 9, 1958.

Journal of Research of the National Bureau of Standards Vol. 62, No. 4, April 1959 Research Paper 2948

Capacity Requirement of a Mail Sorting Device [1]

B. K. Bender and A. J. Goldman

A mathematical model of a sorting device suggested by S. Henig is considered. The relevant parameters are r (the number of destinations for the mail) and k (the number of letters entering the device during each cycle of operation). It is shown that the device will never jam if its capacity is at least $(r-1)(k-1)+k$ letters; this is the lowest possible capacity requirement, and for realistic values of r and k is significantly less than the previously known estimate r^2k.

1. Introduction

We deal with a highly idealized mathematical model of a mail sorting device suggested by S. Henig (NBS Electronic Instrumentation Section). For our purposes, the operation of the device can be described [2] as follows. Mail (to any of r destinations) enters the system. After k letters have entered, the device "asks itself" to which destination it contains the *most* letters.[3] All letters to this *predominant destination* are then *dropped out* of the device, another k letters enter, and the process continues.

The device is said to *jam* if, after a dropout, it is still so "full" that entrance of the next k letters would cause an "overflow". We will determine the minimum capacity required of the device to ensure that no jamming occurs. This is of course equivalent to determining (in terms of r and k) the *maximum possible contents* of the device under the dropout rule described above, and we shall work with this alternative version of the problem. The derivation involves nothing more complicated than counting up letters, so that nonmathematician readers should be able to follow the arguments.

2. Statement of Results

In order to describe our results, it is convenient to define

$$x(t) = \text{number of letters in the device just before the } t\text{th dropout.} \tag{1}$$

A. Bruce Clarke [4] has shown that

$$x(t) \leq r^2k, \text{ for all } t, \tag{2}$$

which proves that the number of letters in the device never exceeds r^2k, so that the device will never jam if its capacity is r^2k or more. Clarke (see footnote 4) remarks that "this upper bound for $x(t)$ is clearly much too crude to be of any practical use;" for example, for the Philadelphia-mail-type data (with $r=200$, $k=3$) used for numerical illustration, it only informs us that the device will never jam if its capacity is 120,000 or more.

As was pointed out by L. S. Joel (NBS Computation Laboratory), the estimate (2) can be very much reduced using rather simple arguments. It will in fact be shown that

$$x(t) \leq (r-1)(k-1)+k, \text{ for all } t, \tag{3}$$

which proves that the number of letters in the device can never exceed $(r-1)(k-1)+k$, so that a capacity of at least $(r-1)(k-1)+k$ will ensure that the device never jams. For the Philadelphia-type data, this shows that a capacity of 401 (rather than 120,000) is sufficient to prevent jamming. The proof of inequality (3) will be given in section 3.

In addition, it will be shown that the device *can* jam if its capacity is *less* than $(r-1)(k-1)+k$; that is, it is possible (under the dropout rule described above) for the number of letters in the device actually to reach $(r-1)(k-1)+k$. In other words, the estimate in (3) is not only an upper bound for $x(t)$ but is the maximum possible value for $x(t)$:

$$x(t)_{\max \text{ poss}} = (r-1)(k-1)+k \tag{4}$$

This will also be proved in section 3. Section 4 contains some comments on the probabilistic aspects of the problem.

3. Proofs

3.1. Proof of Inequality (3)

It is assumed, of course, that the device had fewer than $(r-1)(k-1)+k$ letters in it at the start of operation. An "indirect proof" will be used; that is, we can tentatively suppose that (3) is false and show that this supposition is untenable.

If (3) is false, there must be a first value t_0 of t (i.e., a first dropout) for which it fails. Since (3) is false for $t=t_0$ but true for $t=t_0-1$, we have

$$x(t_0) > (r-1)(k-1)+k, \tag{5}$$

$$x(t_0-1) \leq (r-1)(k-1)+k. \tag{6}$$

[1] Part of a project supported by the Post Office Department, Office of Research and Engineering.

[2] The physical device can also operate under "dropout rules" other than the one described below.

[3] A rule for breaking "ties" between destinations is also required.

[4] A. Bruce Clarke, A mathematical model for the Henig sorting machine, partly abstracted in Ann. Math. Statistics **29**, 622 (1958).

We continue the argument by pointing out two facts about the contents of the device *directly after the* (t_0-1)*-st dropout:*

(a) There are more than $(r-1)(k-1)$ letters in the device, and

(b) There are at least k letters in the device to some one destination.

The truth of (a) follows directly from (5) and the fact that only k letters were added between the (t_0-1)-st and t_0-th dropouts. All letters to some destination left the device in the (t_0-1)-st dropout, so that if (b) were false the device would contain at most $(k-1)$ letters to each of at most $(r-1)$ destinations, or at most $(r-1)(k-1)$ letters in all, contradicting (a). Thus (b) is true.

From (b) and the dropout rule it can be seen that the (t_0-1)-st dropout consisted of at least k letters, so, examining the contents of the device just *before* the (t_0-1)-st dropout, we have

(number of letters to predominant dest.) $\geq k$,

and by (a),

(number of letters to other dest.'s) $>(r-1)\,)k-1)$;

the last two inequalities together yield

$$x(t_0-1)>(r-1)(k-1)+k, \tag{7}$$

which contradicts (6). Thus the supposition that (3) is false is untenable, so (3) must be true.

3.2. Proof of Equation (4)

We already know, by (3), that the device can never contain *more* than $(r-1)(k-1)+k$ letters. Thus, in order to prove (4), it suffices to exhibit a sequence of possible events leading to a situation in which the device contains *exactly* $(r-1)(k-1)+k$. There are many such sequences, and the one described below is not necessarily the shortest one.

The sequence will be constructed in two stages, beginning with the device empty at $t=0$. At the end of stage 1, the device will contain $k-1$ letters to each of 2 destinations and $k-2$ letters to each of the other $r-2$ destinations. At the end of stage 2, the device will contain exactly $(r-1)(k-1)+k$ letters and the proof of equation (4) will have been completed.

Stage 1: We suppose that the r destinations are numbered in some way. The sequence of possible events begins as follows: [5] The first k letters entering the device consist of one letter to the first destination and $k-1$ letters to the rth destination; these last $(k-1)$ letters then leave the device in the first dropout. The second k letters to enter the device consist of one letter to the second destination and $k-1$ letters to the rth destination, etc. After the $(r-1)$-st dropout, the device contains no letters to the rth destination and one letter to each other destination. The rth set of k letters to enter the device consists of one letter to the first destination and $k-1$ letters to the rth destination, and the process continues as before; after the $(r-1)(k-2)$-nd dropout the device contains no letters to the rth destination and $k-2$ letters to each of the $(r-1)$ other destinations.

The k letters entering the device between the $(r-1)(k-2)$-nd and $((r-1)(k-2)+1)$-st dropouts consist of $k-1$ letters to the rth destination and one letter to some other destination; the device now contains $k-1$ letters to each of 2 destinations and $k-2$ letters to each of the other $r-2$ destinations. In other words, if we define

$$\left.\begin{array}{l} n(t)=\text{number of destinations to which there are} \\ \quad k-1 \text{ letters in the device just before the} \\ \quad t\text{th dropout,} \end{array}\right\} \tag{8}$$

then we have

$$n((r-1)(k-2)+1)=2. \tag{9}$$

The $((r-1)(k-2)+1)$-st dropout will consist of $k-1$ letters to whichever of the 2 destinations mentioned above is "preferred" by whatever tie-breaking rule is employed. After this dropout the device will contain no letters to some one destination, $k-1$ letters to some other destination, and $k-2$ letters to each of the $r-2$ remaining destinations.

Stage 2: In this stage matters will be arranged so that

$$\text{for } \begin{array}{c} n(t)=n(t-1)+1 \\ (r-1)(k-2)+2\leq t\leq (r-1)(k-1); \end{array} \tag{10}$$

i.e., so that after each dropout there are $k-1$ letters in the device to *one more* destination than before. If this is done, then by (9) and repeated application of (10) we have

$$n((r-1)(k-1))=n((r-1)(k-2)+(r-1))=r,$$

so that just before the $(r-1)(k-1)$-st dropout the device contains $k-1$ letters to each of the r destinations. Then $k-1$ of these $r(k-1)$ letters are dropped leaving $(r-1)(k-1)$ in all, and k new letters enter; the device now contains $(r-1)(k-1)+k$ letters, and equation (4) is proved.

To achieve (10) we choose the k letters entering the device between the $(t-1)$-st and tth dropouts, for $t=(r-1)(k-2)+2,\ (r-1)(k-2)+3,\ \ldots,\ (r-1)(k-1)$, to consist of $k-1$ letters to the destination just previously dropped out, and one letter to a destination which previously had $k-2$ letters to it in the device.

4. Probabilistic Aspects of the Capacity Problem

We have been concerned above with choosing the capacity of the device so that jamming *never* occurs. In practice we might well have the more modest aim of keeping the frequency of jamming down to some tolerable level, and so could get by with a

[5] For a more formal description of the following process, let $R(t)$ denote the remainder when t is divided by $r-1$, except that $R(t)=r-1$ when t is a multiple of $r-1$. The for $1\leq t\leq (r-1)(k-2)$, the k letters entering the device between the $(t-1)$-st and tth dropouts are to consist of one letter to the $R(t)$-th destination and $k-1$ letters to the rth destination.

smaller capacity than that indicated by eq (4). On the one hand this leads to the "policy" question of what jamming frequencies are to be considered intolerable; on the other hand, it leads to the purely mathematical problem of what capacity is needed in order to keep jamming below these frequencies.

This last problem seems very difficult. As was pointed out (unpublished memorandum, July 1956) by J. R. Rosenblatt (NBS Statistical Engineering Laboratory), the behavior of the device constitutes a stochastic process (indeed, a Markov chain) governed by the probabilistic distribution of mail by destinations. The possible number of "states" of the device is very large (for realistic values of r and k), and the creation of analytic techniques for the treatment of Markov chains with a great many states appears to be one of the "underdeveloped areas" of applied mathematics. We know that the specific Markov chain in the current problem has a probabilistic "steady state" toward which the device "settles down," and the *average* number $E(x)$ of letters in the device before dropouts, in this steady state, might serve as a very rough initial guide [6] to the capacity required of the device. Even the determination of $E(x)$ seems far from easy; we may note that the upper bound derived for $E(x)$ by a complicated probabilistic argument (see reference cited in footnote 4) yields the result $E(x) \leq 545$ for the particular illustrative data used, whereas our eq (4) (which was not aimed at estimating $E(x)$ and does not use the probabilistic distribution of mail by destinations) can be combined with the inequality

$$E(x) \leq x(t)_{\text{max poss}}$$

to yield the sharper result $E(x) \leq 401$ for the same data.

[6] The frequency of large-amplitude oscillations around this average must also be considered; at the very least, some information is required on the standard deviation of the number of letters in the device.

WASHINGTON, January 5, 1959.

Journal of Research of the National Bureau of Standards Vol. 62, No. 4, April 1959 Research Paper 2949

Effect of Internal Radiant Heat Transfer on Temperature Distribution, Thermal Stress, and Deflection in Box Beams [1]

Stanley Goodman, Stanton B. Russell, and Charles E. Noble

Thirteen box beams were analyzed to determine the effect of internal radiant heat transfer on temperature distribution, thermal stress, and deflection. A rough experimental check of temperature distribution and beam deflection was made for one case. For maximum beam temperatures above 700° to 900° F, change in emittance of the interior surfaces of the beam had an appreciable effect on the cover (but not the web) temperatures and to an even greater extent, on the beam deflection. At maximum beam temperatures of 1,200° F, an increase in interior surface emittance appreciably relieved the maximum thermal stress.

1. Introduction

The subjection of aircraft and other structures to increasingly high temperatures gives rise to a need for predicting the transient temperature distribution in the structures, and the resulting thermal stresses and deformations. This knowledge will make possible the rational design of the structure, and the devising of methods of alleviating thermal stresses and deflections.

As the temperature of a structure increases, radiation becomes more important as a mode of heat transfer [1].[2] The influence of radiant heat transfer on the temperature distribution of the structure is affected by structural geometry, heating rate, and thermal properties of the beam material. The purpose of this investigation was to determine the effect of changing the emittance of the interior surfaces of a box beam on temperature distribution, maximum thermal stress, and beam deflection in heated box beams.

2. Structures and Material

Thirteen analyses were made of modifications of three basic types of box beams. The beam cross sections are shown in the figure at the top of table 1; wall thicknesses are indicated by the ratios listed in columns 2 and 3 of the table. One type (cases 1, 2, and 3) is a thick-walled beam, similar to a beam used in the experimental work. The other types are typical of beams used in aircraft structures; one type is relatively thick-walled (cases 4 to 8) and the other relatively thin-walled (cases 9 to 13).

Thermal and elastic properties were taken as those of the type 302 stainless-steel test beam. Thermal conductivity and specific heat were approximated by the linear relationships:

$$k=7.08+0.0043T \tag{1}$$

$$c=0.106+0.0000257T, \tag{2}$$

where k is thermal conductivity (Btu/hr ft ° F); c is specific heat (Btu/lb ° F); and T is absolute temperature (° R). Hemispherical total emittance was taken as 0, 0.35 (emittance of the test beam, cases 1 to 3) and 1, as indicated in columns 4 and 5 of table 1.

Young's modulus and the coefficient of linear thermal expansion were represented by

$$E=31.0\times10^6-0.0064T\times10^6 \tag{3}$$

$$\alpha=8.29\times10^{-6}+0.00137T\times10^{-6}, \tag{4}$$

where E is Young's modulus (lb/in.^{2}), α is coefficient of linear thermal expansion (in./in. ° F), and T is absolute temperature (° R).

3. Boundary Conditions

The beams were assumed to be subjected to a uniform heat input along one cover in a rarefied atmosphere. The heating rates are listed in columns 6 and 7 of table 1. The initial beam temperature was assumed to be 78° F. For the test beam (cases 1, 2, 3), the boundary condition was taken as the heated cover temperature (figs. 2 and 7) observed in an experiment. For all other cases, the boundary condition was taken as the assumed heat input to the cover. All elements of the heated cover were assumed to remain constant at 1,200° F after reaching that temperature.

4. Method of Analysis

4.1. Calculation of Temperature Distribution

Analysis was made by a numerical method similar to that described by Dusinberre [2]. The beam cross section was divided into analysis elements, and a heat-balance equation was set up for each analysis element and solved for the element temperature after a short time interval, $\Delta\theta$. The process was repeated for successive short-time intervals using the new element temperatures as the starting point of the next computation. It

[1] This work was conducted at the National Bureau of Standards under the sponsorship and with the financial assistance of the Office of Naval Research.
[2] Figures in brackets indicate the literature references at the end of this paper.

TABLE 1. *Computed cover temperatures, maximum thermal stress and maximum deflection in box beams heated along one cover*

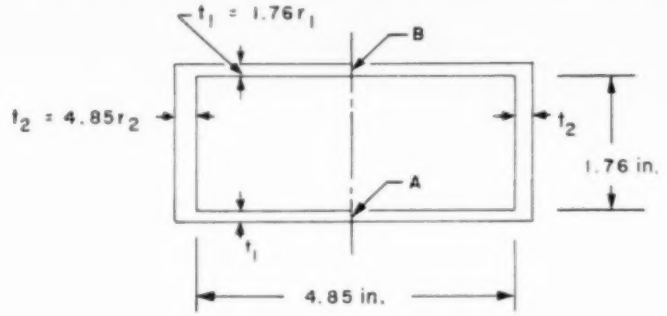

Case	r_1	r_2	Surface emittance		Heating rate		Elapsed time	Temperature [b] at		Maximum stress [c]		Maximum deflection [c d]
			Interior	Exterior				*A*	*B*	Tensile	Compressive	
					Btu/hr ft²	*°F/sec* [a]	*sec*	*° F*	*° F*	*psi*	*psi*	*in./in.²*
1	0.0727	0.0264	0	0.35	-----	3.8	378	958	84	35.3×10^3	29.3×10^3	0.46×10^{-2}
2	.0727	.0264	0.35	.35	-----	3.8	378	958	147	35.8	29.7	.42
3	.0727	.0264	1	.35	-----	3.8	378	958	377	34.8	30.5	.30
4	.02	.03	0	.35	32400	50	26.6	1202	78	121.7	127.9	.49
5	.02	.03	0.35	.35	32400	50	26.6	1173	101	118.0	124.4	.47
6	.02	.03	1	.35	32400	50	26.6	1095	188	108.5	116.1	.41
7	.02	.03	0.35	0	32400	50	26.6	1200	102	121.5	127.1	.48
8	.02	.03	.35	1	32400	50	26.6	1104	98	111.0	116.7	.44
9	.01	.01	0	0.35	10800	30	45	1204	78	102.9	99.0	.58
10	.01	.01	0.35	.35	10800	30	45	1135	154	92.1	91.0	.51
11	.01	.01	1	.35	10800	30	45	959	371	71.5	74.9	.34
12	.01	.01	0	.35	32400	91	13.7	1200	78	127.6	101.1	.58
13	.01	.01	1	.35	32400	91	13.7	1125	203	114.5	95.1	.49

[a] Approximate temperature rise rate at point *A* up to about 800° F.
[b] Initial temperature 78° F.
[c] Neglecting yielding, creep, and buckling.
[d] Deflection per unit beam length squared.

was assumed that surface emittance remained constant and that beam surfaces reflected diffusely and were gray, i.e., total emittance and absorptance are equal at all beam temperatures. Gaseous heat transfer was neglected.

One-half of the cross section of the symmetrical beam was divided into 12 analysis elements. Since the external heat transfer was symmetrical with respect to the left and right halves of the beam cross section, the right half of the beam was represented by a perfect but diffuse reflector. The reflector was divided into four regions. The element configuration for cases 1, 2, and 3, shown in figure 1, is typical of all cases.

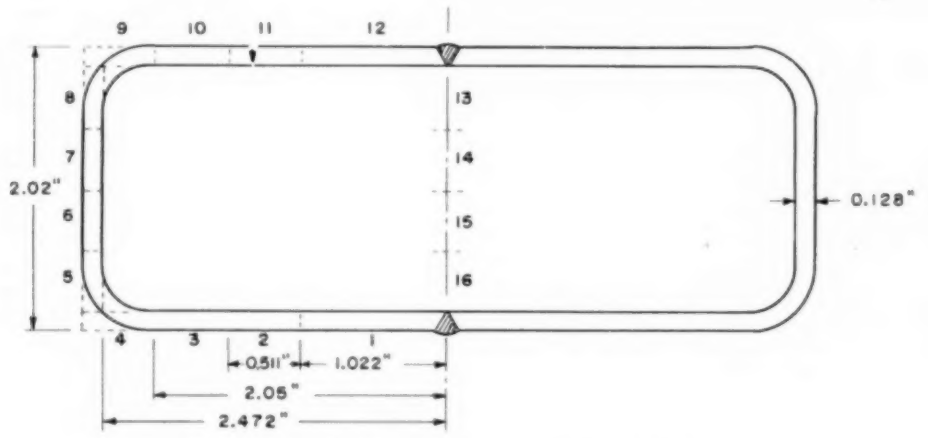

FIGURE 1. *Test beam cross section (cases 1, 2, 3).*

Material: Stainless steel, 18-8 (302); length: 30 in.; analysis elements designated by dotted lines and small numerals.

The heat balance equation is as follows:

$$T'_m = T_m + \frac{\Delta\theta}{V_m \rho C_m}\Big\{ (k_{m-1,m})(H_m)(T_{m-1}-T_m) + (k_{m,m+1})(J_m)(T_{m+1}-T_m) + \epsilon_m \sigma A_m (T_A^4 - T_m^4) + \sigma A'_m [F_{m,1}(T_1^4 - T_m^4) + F_{m,2}(T_2^4 - T_m^4) + \cdots + F_{m,12}(T_{12}^4 - T_m^4)] + W_m \Big\},$$

where

T'_m is the temperature (°R) at the center of element m after time interval $\Delta\theta$

V_m is the volume (ft^3) of element m

T_m is the temperature (° R) at the center of element m at the beginning of the time interval $\Delta\theta$

ρ is the density of the material (lb/ft^3)

C_m is the specific heat of element m (Btu/lb ° F), represented by a linear function of T_m.

$k_{m,\,m+1}$, $k_{m-1,\,m}$, are the thermal conductivities of the beam metal at the mean temperatures of the elements m and $m+1$, and m and $m-1$, respectively (Btu/hr ft ° F)

H_m, J_m are ratios of element contact areas to distances between element centers for element m and adjacent elements $m-1$, $m+1$, respectively (ft)

ϵ_m is hemispherical total emittance of element surface m

σ is the Stefan-Boltzmann constant (0.1713×10^{-8}) in Btu/ft^2 hr ° R^4

A_m is exterior surface area (ft^2) of element m

T_A is ambient temperature (° R)

A'_m is interior surface area (ft^2) of element m

$F_{m,n}$ is an over-all radiant heat interchange factor for net radiant heat exchange between a gray surface of element m and a gray surface of element n. It includes the effect of direct and all reflected radiation.

W_m is the external heat input (Btu/hr).

The first two terms inside the brackets on the right-hand side of eq (5) represent conductive heat transfer between element m and adjacent elements; the third term represents radiant heat transfer with the outside environment, the fourth term represents internal radiant heat exchange between element m and the rest of the beam interior; the fifth term represents the assumed heat input boundary condition. For cases 1, 2, and 3 in which the boundary condition was taken as the observed heated cover temperature history of the test beam, the temperature of each heated cover element was expressed by four linear functions of time covering successive time intervals.

To compute the graybody radiant heat exchange factors, F, blackbody radiant heat exchange factors were computed for all two-element combinations of the 16 internal surfaces of the analysis elements and (fictitious) reflector using the methods of reference [3], and radiation geometry. Values of the 256 F's were then obtained from the matrix relationships of reference [4]. The computations were performed on SEAC using an existing code for inverting the matrices.

The temperature-distribution computations were computed on SEAC. Temperatures at the midpoints of the 12 analysis elements of the beam were printed out at regular time intervals which were whole number multiples of $\Delta\theta$.

In order to minimize computing machine running time, it was desirable to use the largest value of the time interval, $\Delta\theta$, consistent with adequate accuracy of solution. The time interval must be sufficiently short that during the interval (1) The initial element temperatures can be used with negligible error and (2) for conductive heat transfer; the effect of any nonadjacent element on a given element is negligible. Satisfactory values of $\Delta\theta$ were obtained by trial. A portion of the temperature distribution history was computed several times using successively larger values of $\Delta\theta$. The largest value of $\Delta\theta$ which gave a temperature distribution history negligibly different from that obtained with the smallest value of $\Delta\theta$ was used to compute the complete temperature distribution history. Values of $\Delta\theta$ found satisfactory by this method ranged from 0.72 sec for rapidly heated beams to 1.8 sec for slowly heated beams.

Some error was generated in the beam temperature history computations by representing one-half of the beam cross section by a perfect, diffuse rather than specular, reflector. As a check on the magnitude of this error, radiant heat transfer rates were computed for a simple symmetrical case using first the entire beam cross section in the computations, and then an equivalent beam consisting of one-half of the beam cross section and a diffuse reflector. An infinitely long box beam of rectangular cross section divided into six analysis elements was used. The beam was 2-in. deep, 8-in. wide, and emissivity was 0.35. The vertical (2-in.) walls of the beam were at temperature T_1 and the horizontal walls at absolute zero. The rate of radiant heat transfer to the left half of the upper horizontal wall was

$$q = 0.1354\sigma T_1^4 \quad \text{for original beam}$$

$$q = 0.1389\sigma T_1^4 \quad \text{for equivalent beam with diffuse reflector,} \qquad (6)$$

where q is rate of radiant heat transfer (Btu/hr ft^2); σ is the Stefan-Boltzmann constant (0.1713×10^{-8} Btu/(ft^2 hr ° R^4)); and T_1 is vertical wall temperature (° R). It was concluded that the error due to use of a diffuse rather than a specular reflector was small.

4.2. Computation of Thermal Stress and Deflection

Thermal stresses and deflections in the beam were computed by the methods described in reference [5]. Integrations over the beam cross section were performed numerically using finite elements identical

with those used in the temperature distribution computations (fig. 1). Possible effects of yielding, creep, and buckling were neglected.

5. Test of Beam

The test specimen, corresponding to case 2, table 1, was a box beam constructed of 0.128-in.-thick type 302 stainless-steel sheet (fig. 1). Two pieces of sheet were each bent into identical channel shapes and butt welded together lengthwise to form the 2 in. by 5 in. by 30 in. beam.

The beam was heated in a vacuum chamber whose pressure was maintained at 4 mm of mercury, a pressure low enough to eliminate appreciable convective heat transfer. Only one cover of the beam was subjected to heating. It was heated with 12 quartz-tube, tungsten-filament heating elements uniformly spaced in a reflector. Total output of the heaters was 5.7 Btu/sec. The reflector, a rectangular silver-plated stainless-steel channel enclosing the heating elements, confronted the heated cover of the beam. The reflectance of the reflector surface was about 0.97.

Temperatures were measured at the center cross section on the heated cover of the beam, at the center cross section on the unheated cover, at two points on the heated cover 1 in. from one end, and at one point on the heated cover 1 in. from the other end. The temperatures were measured with iron-constantan thermocouples whose outputs were indicated by galvanometers. The thermocouples were calibrated before and after the test. The temperature rise of the heated cover was approximately 12 percent less at the beam ends than at the center cross section. The experimentally determined heated cover temperatures, which were used as the boundary condition in cases 1, 2, and 3, are shown in figure 2 and, together with observed temperatures for two points on the opposite cover, in figure 7.

The normal total emittance of the type 302 stainless steel was determined by comparing its rate of radiation at a given temperature with that of a silicon carbide bar at the same temperature. The radiation rates were determined by focusing the images of equal areas of the silicon carbide bar and of the stainless steel successively on a thermopile, using a fluorite lens. The emittance of the stainless steel obtained was constant in the temperature range 400° to 1,000° F and equal to 0.35.

Beam deflection at the center cross section was measured by means of SR–4 type AB–5 electrical strain gages mounted back-to-back on a shielded cantilever beam which was deflected by displacement of the center of the beam relative to its ends. Contact of the center of the beam with the cantilever was made by a Vycor rod. Calibration was accomplished by deflecting the cantilever by known amounts at the point of contact with a micrometer screw.

The maximum deflection observed was 0.415 in. after 240 sec of heating. After 378 sec of heating the center deflection was 0.37 in.

6. Results

6.1. Beam-Temperature Distribution

Computed temperature histories at point A, in the center of the heated cover and at point B, in the center of the opposite cover (see sketch on table 1) are shown in figures 2 to 6 for the 13 cases considered. Figure 7 shows the computed temperature distribution in a thick-walled beam (cases 1, 2, 3) of the same dimensions as the test beam after 148, 189, and 297 sec of heating. Figure 8 shows the temperature distribution in a thin-walled beam after 45 sec of slow heating, and after 13.7 sec of fast heating. Temperatures at A and B are listed in columns 9 and 10 of table 1. Comparison was made of geometrically similar beams heated at the same rate for the same length of time but having the following different values of interior or exterior emittances: 0, 0.35, and 1.0.

It was found that, in all cases considered, a change in emittance of the surfaces had an appreciable effect on the cover temperatures and little on the web temperatures when the maximum heated cover temperature was above 700° to 900° F. For beams with the heated cover at a temperature of about 1,200° F, changing the internal emittance from 0 to 1.0 reduced the temperature difference, d, between points A and B by 18 percent for the thin-walled beam with the cover heated at 91° F/sec, and by 48 percent for the same beam with one cover heated at 30° F/sec. For the same cover-heating rate the effect of change in interior emittance was less for the thicker-walled beam.

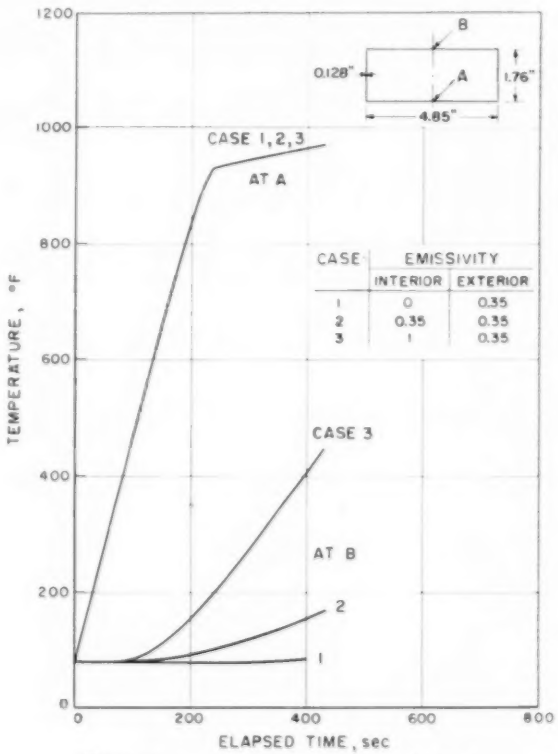

FIGURE 2. *Beam temperature history.*

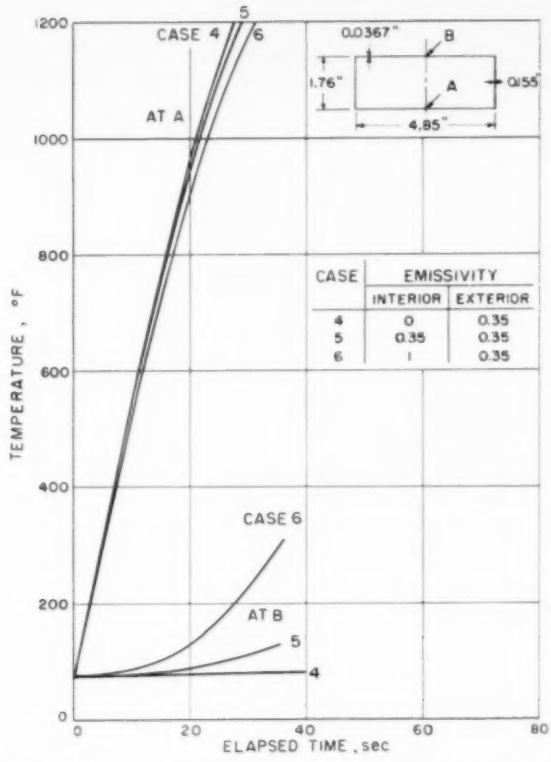

FIGURE 3. *Beam temperature history for heating rate of 32,400 Btu/hr ft².*

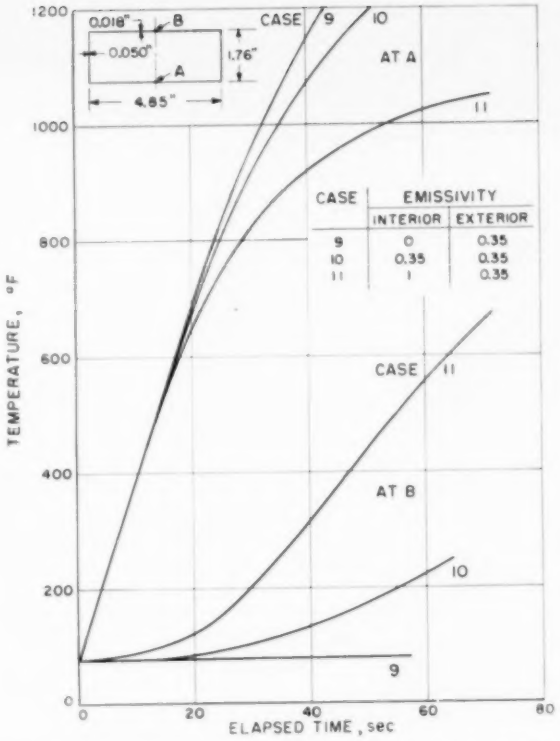

FIGURE 5. *Beam temperature history for heating rate of 10,800 Btu/hr ft².*

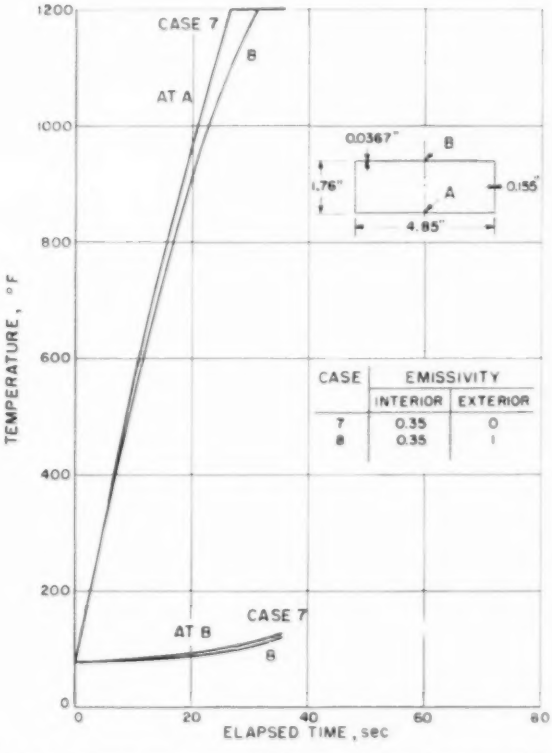

FIGURE 4. *Beam temperature history for heating rate of 32,400 Btu/hr ft².*

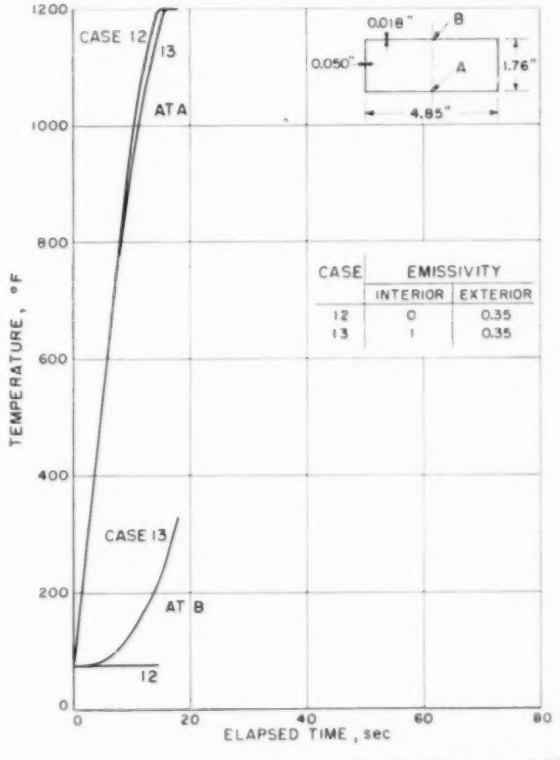

FIGURE 6. *Beam temperature history for heating rate of 32,400 Btu/hr ft².*

A change in exterior surface emittance has less effect on d than a change in interior surface emittance. Comparison of cases 4 and 6 with corresponding cases 7 and 8 indicates that, for the particular conditions specified in table 1, increasing the interior surface emittance from 0 to 1.0 causes a decrease in d of 19 percent; increasing the exterior surface emittance from 0 to 1.0 causes a decrease in d of only 8 percent.

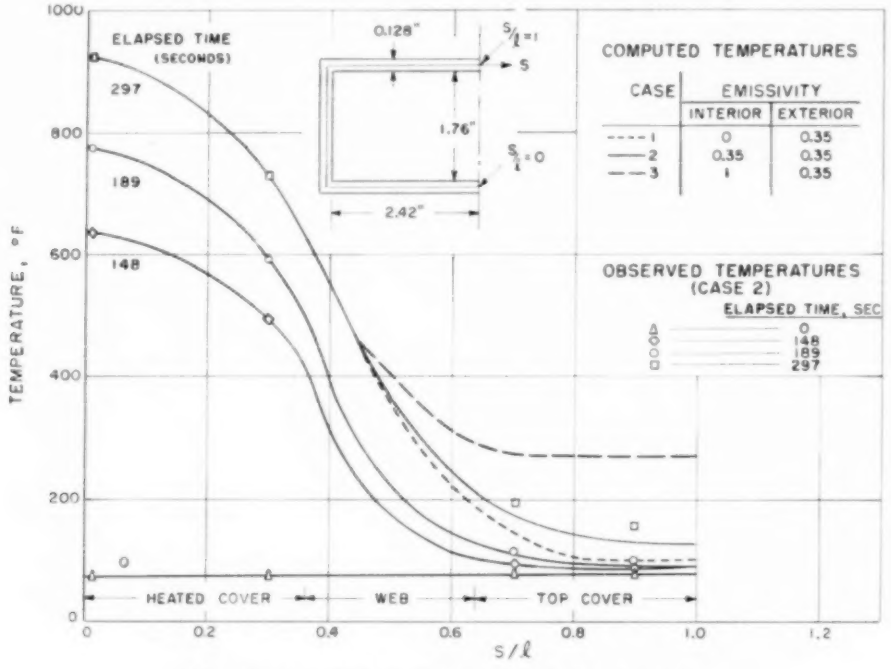

FIGURE 7. *Test beam temperature distribution.*

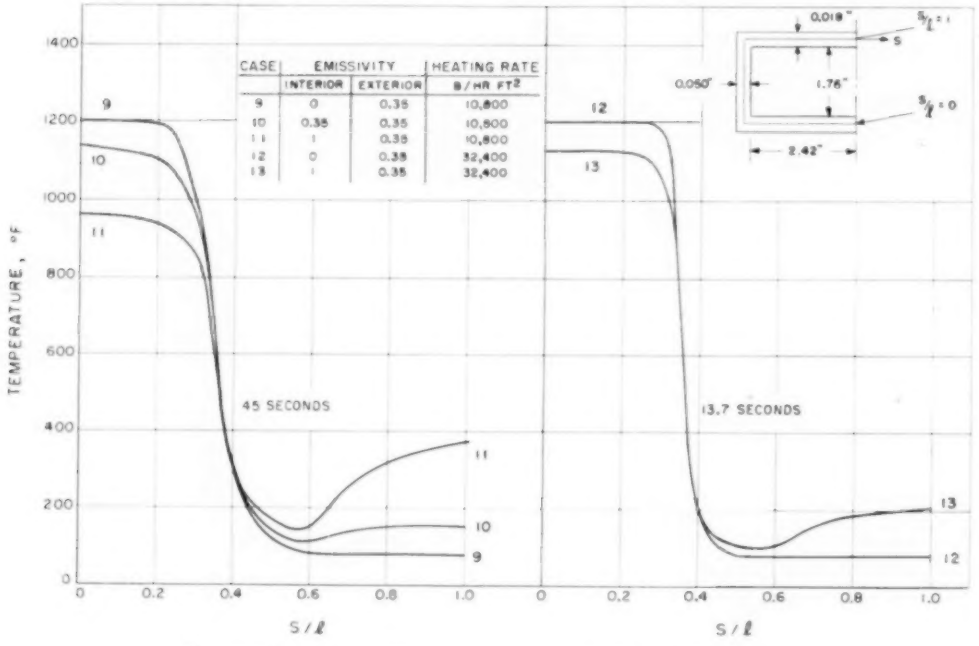

FIGURE 8. *Temperature distribution in thin-walled beam.*

6.2. Thermal Stress and Deflection

In order to evaluate the effect of a change in emittance on the thermal stress distribution and deflection, thermal stress distributions and deflections were computed for the 13 cases under the conditions listed in table 1. Maximum tensile stress, maximum compressive stress, and maximum deflection are listed in columns 11, 12, and 13, respectively, in the table. To generalize the results as regards beam length the deflection is given as the deflection per unit beam length squared; the maximum deflection is proportional to the beam length squared, the thermal stresses are independent of the beam length. The possible effects of yielding, creep, and buckling were neglected. Values of the thermal stress and deflection are therefore valid only for comparison purposes.

For a thick-walled, slowly heated beam with heated cover at 958° F (cases 1, 2, 3) a change in the interior wall emittance has little effect on the magnitude of the maximum thermal stress. An increase in the interior wall emittance from 0 to 1.0 however, results in a decrease of 34 percent in the maximum beam deflection. For the beams with the same geometry and under the same heating conditions in which the final heated cover temperature is about 1,200° F, a change of the interior wall emittance from 0 to 1.0 reduces the absolute maximum stress by from 9 percent (cases 4 and 6) to 27 percent (cases 9 and 11), and deflection by from 15 percent (cases 12 and 13) to 40 percent (cases 9 and 11). In the latter beam, the reduction in maximum tensile stress was 31 percent. For a change of the exterior wall emittance from 0 to 1.0 (cases 7 and 8), the reduction in absolute maximum stress was 8 percent, and the reduction in maximum deflection was 7 percent.

For the beams analyzed, changing the interior beam emittance from 0.35 to 1 causes a change in the temperature difference, d, between A and B which is about 75 percent of the change that would occur for a change in emittance from 0 to 1. Corresponding ratios for maximum thermal stress and deflection are about 66 and 74 percent, respectively.

6.3. Comparison of Experimental and Theoretical Results

A partial check of the temperature distribution and deflection was made for case 2 using a beam 30 in. long. Computed and observed temperatures for two points on the unheated cover after 148, 189, and 297 secs of heating are shown in figure 7. Agreement is fair. Some of the discrepancy may be attributed to gas heat transfer within the beam. For the conditions listed under case 2 in table 1, observed beam deflection was 0.37 in. and beam deflection computed from the theoretical temperature distribution was 0.38 in. i.e., 0.00042 in./(in. length)^2.

7. Conclusions

A change in the interior surface emittance of a box beam heated along one cover has an appreciable effect on the temperature distribution, and consequently on the maximum thermal stress and the deflection. For a variety of beam geometries and heating conditions, a change of the interior surface emittance from 0.35 to 1 for a stainless steel beam reduces considerably the temperature difference from cover to cover in the temperature range above 700° to 900° F and the maximum thermal stress and the deflection in the temperature range above 900° to 1,200° F. The effect is particularly marked for a thin-walled slowly-heated beam.

8. References

[1] S. Goodman, Radiant-heat transfer between nongray parallel plates, J. Research NBS **58,** 37 (1957) RP2732.

[2] G. M. Dusinberre, Numerical methods for transient heat flow, Trans. ASME **67,** 703–712 (1945).

[3] D. C. Hamilton and W. R. Morgan, Radiant interchange configuration factors, NACA TN 2836 (December 1952).

[4] W. H. McAdams, Heat transmission, 3d ed. (McGraw-Hill Book Co., Inc., New York, N.Y., 1954).

[5] S. Levy, Thermal stresses and deformations in beams, Aeronaut. Eng. Rev. **15,** 62–70 (1956).

WASHINGTON, December 2, 1958.

Important Notice

Beginning in July 1959, the Journal of Research will be published in four separate sections which may be subscribed for individually. This change is being made to provide a publication whose subject matter concentrates on particular fields of interest, thus meeting the specialized needs of individual scientists, engineers, and mathematicians.

Section A. Physics and Chemistry, to be issued bimonthly, will present papers of interest primarily to scientists working in these fields. This section will cover a broad range of physical and chemical research, with major emphasis on standards of physical measurement, fundamental constants, and properties of matter.

Section B. Mathematics and Mathematical Physics, to be issued quarterly, will present results in pure and applied mathematics, including mathematical statistics, theory of experiment design, numerical analysis, and short numerical tables; theoretical physics, chemistry, and engineering, where the emphasis is on the mathematical content or methodology; and logical design, programing, and applications of electronic computers and computer systems.

Section C. Engineering and Instrumentation, to be issued quarterly, will report results of interest chiefly to the engineer or applied scientist. This section will include many of the new developments in instrumentation resulting from the Bureau's work in physical measurement, data processing, and the development of test methods. It will also cover some of the work in acoustics, applied mechanics, building research, and cryogenic engineering.

Section D. Radio Propagation, to be issued bimonthly, will report research in radio propagation, communications, and upper atmospheric physics. Topics to be covered include propagation in ionized media, scattering by turbulence, the effect of irregular terrain on propagation, diffraction and scattering by solid obstacles, propagation through time-varying media, and antennas.

All present subscribers to the Journal will receive an announcement from the Superintendent of Documents when advance orders for the new sections can be accepted.

THE NATIONAL BUREAU OF STANDARDS

The scope of activities of the National Bureau of Standards at its headquarters in Washington, D.C., and its major laboratories in Boulder, Colorado, is suggested in the following listing of the divisions and sections engaged in technical work. In general, each section carries out specialized research, development, and engineering in the field indicated by its title. A brief description of the activities, and of the resultant publications, appears on the inside of the front cover.

WASHINGTON, D. C.

Electricity and Electronics. Resistance and Reactance. Electron Devices. Electrical Instruments. Magnetic Measurements. Dielectrics. Engineering Electronics. Electronic Instrumentation. Electrochemistry.

Optics and Metrology. Photometry and Colorimetry. Optical Instruments. Photographic Technology. Length. Engineering Metrology.

Heat. Temperature Physics. Thermodynamics. Cryogenic Physics. Rheology. Engine Fuels. Free Radicals Research.

Atomic and Radiation Physics. Spectroscopy. Radiometry. Mass Spectrometry. Solid State Physics. Electron Physics. Atomic Physics. Neutron Physics. Radiation Theory. Radioactivity. X-rays. High Energy Radiation. Nucleonic Instrumentation. Radiological Equipment.

Chemistry. Organic Coatings. Surface Chemistry. Organic Chemistry. Analytical Chemistry. Inorganic Chemistry. Electrodeposition. Molecular Structure and Properties of Gases. Physical Chemistry. Thermochemistry. Spectrochemistry. Pure Substances.

Mechanics. Sound. Mechanical Instruments. Fluid Mechanics. Engineering Mechanics. Mass and Scale. Capacity, Density, and Fluid Meters. Combustion Controls.

Organic and Fibrous Materials. Rubber. Textiles, Paper Leather. Testing and Specifications. Polymer Structure. Plastics. Dental Research.

Metallurgy. Thermal Metallurgy. Chemical Metallurgy. Mechanical Metallurgy. Corrosion. Metal Physics.

Mineral Products. Engineering Ceramics. Glass. Refractories. Enameled Metals. Concreting Materials. Constitution and Microstructure.

Building Technology. Structural Engineering. Fire Protection. Air Conditioning, Heating, and Refrigeration. Floor, Roof, and Wall Coverings. Codes and Safety Standards. Heat Transfer.

Applied Mathematics. Numerical Analysis. Computation. Statistical Engineering. Mathematical Physics.

Data Processing Systems. SEAC Engineering Group. Components and Techniques. Digital Circuitry. Digital Systems. Analog Systems. Application Engineering.

• Office of Basic Instrumentation.

• Office of Weights and Measures.

BOULDER, COLORADO

Cryogenic Engineering. Cryogenic Equipment. Cryogenic Processes. Properties of Materials. Gas Liquefaction.

Radio Propagation Physics. Upper Atmosphere Research. Ionospheric Research. Regular Propagation Services. Sun-Earth Relationships. VHF Research. Ionospheric Communication Systems.

Radio Propagation Engineering. Data Reduction Instrumentation. Modulation Systems. Navigation Systems. Radio Noise. Tropospheric Measurements. Tropospheric Analysis. Radio Systems Application Engineering. Radio-Meteorology.

Radio Standards. High Frequency Electrical Standards. Radio Broadcast Service. High Frequency Impedance Standards. Electronic Calibration Center. Microwave Physics. Microwave Circuit Standards.

Recent Publications of the National Bureau of Standards

Periodicals

Journal of Research of the National Bureau of Standards. Volume 62, No. 2, February 1959 (RP2929 to RP2934 incl.). 60 cents.

Technical News Bulletin, Volume 43, No. 2, February 1959. 15 cents. Annual subscription $1.50. 75 cents additional for foreign mailing.

Basic Radio Propagations Predictions for May 1959. Three months in advance. CRPL-D 174. Issued February 1959. 10 cents. Annual subscription $1.00. 50 cents additional for foreign mailing.

Circulars

C563, 1st Supplement. Periodicals and serials received in the library of the National Bureau of Standards, August 1958. 10 cents.*

Miscellaneous Publications

M226. Research highlights of the National Bureau of Standards—Annual Report 1958. 45 cents.*

Available from the Superintendent of Documents, U.S. Government Printing Office, Washington 25, D.C. The Technical News Bulletin and Basic Radio Propagation Predictions are available on a 1-, 2-, or 3-year subscription basis, although no reduction in rates can be made.

**Foreign postage, one-fourth additional.*

UNITED STATES
GOVERNMENT PRINTING OFFICE
DIVISION OF PUBLIC DOCUMENTS
WASHINGTON 25, D.C.

OFFICIAL BUSINESS

PENALTY FOR PRIVATE USE TO AVOID PAYMENT OF POSTAGE, $300 (GPO)

Journal of Research of the National Bureau of Standards Vol. 62, No. 4 April 1959

Contents

Page

Interferometer for large surfaces. James B. Saunders and Franz L. Gross. RP2943 137

Glass formation in polymers: II. The system rubber-sulfur. Gordon M. Martin and Leo Mandelkern. RP2944 141

Elastic deformations in strips with holes loaded through pins. Michael Chi and L. K. Irwin. RP2945 147

Absolute light-scattering photometer: I. Design and operation. Donald McIntyre and G. C. Doderer. RP2946 153

Resolution of the dissociation constants of *d,l*-malic acid from 0° to 50° C. Murray Eden and Roger G. Bates. RP2947 161

Capacity requirement of a mail sorting device. B. K. Bender and A. J. Goldman. RP2948 171

Effect of internal radiant heat transfer on temperature distribution, thermal stress, and deflection in box beams. Stanley Goodman, Stanton B. Russell, and Charles E. Noble. RP2949 175

IMPORTANT NOTICE

Beginning in July 1959, the Journal of Research will be published in four separate sections. See the announcement given on the last page of this issue.

[A list of recent NBS publications is given on page 3 of the cover]

For sale by the Superintendent of Documents, U.S. Government Printing Office, Washington 25, D.C. Price 60 cents (single copy)

UNITED STATES GOVERNMENT PRINTING OFFICE, WASHINGTON : 1959